

## Computational Study of Airflow and Dispersion of Airborne Pathogens Inside an Aircraft Cabin

 Raposo, C. L. S.;  Sousa, J. M. M.

IDMEC, Instituto Superior Técnico, Universidade de Lisboa, Av. Rovisco Pais, 1049-001 Lisboa, Portugal

### Abstract

To aid the prevention and mitigation of the next pandemic, aircraft cabins must be continuously designed to ventilate effectively any contaminant dispersed in the air, and eventually allowing the early detection of an event of pathogen spreading. A RANS simulation, employing a modified  $k-\epsilon$  approach and involving a detailed diffuser geometry, was used to accurately simulate the complex behavior of the ventilation jets and compare the results obtained with available experimental data. Subsequently, a contaminant was continuously injected into the center and side of the cabin, and ultimately conjugated with the use of gaspers. Briefly, it was found that, if gaspers are normal to the wall, the conjugated effect with the moist air flow vortex and thermal plume creates a condition of still air, thereby promoting diffusion and decreasing dispersion.

**Keywords:** aircraft cabin; contaminant dispersion; HVAC; RANS simulation.

### 1. Introduction

As a consequence of the ongoing Covid-19 pandemic, governments have imposed severe lockdowns and travel restrictions. During these periods in 2020, about two thirds of the global commercial aircraft fleet were grounded [1]. Despite the visible recovery in flight numbers during 2021, mainly fueled by the air cargo industry, revenue-passenger-kilometers remained below the half of those numbers recorded in recent pre-pandemic years [2]. Implemented measures, such as mass vaccination in several countries throughout the world and the deployment of digital certifications certainly helped to boost travel during the summer of 2021. However, a sustained traffic recovery in coming years will strongly rely on ensuring healthy cabin environments as well as on the reinforcement of control procedures in future epidemics. With this goal in mind, a better knowledge of the airflow mechanisms inside aircraft cabins, together with an improved understanding of the resulting aerosol dispersion patterns appears to be crucial, as droplets and micro-particles released into the air by sick passengers via sneezing, coughing and breathing have been identified as sources of several diseases [3]. A full characterization of these situations is nevertheless complicated by the dimensions and geometrical complexities of the cabin (especially the diffuser), the unsteadiness and instability often exhibited by the airflow, as well as the variability and intricacies associated to the analysis of aerosol dispersion from multiple origins.

Aiming to conduct numerical simulations of the aforementioned problem, a cabin model has been constructed based on the Kansas State University Boeing 767 mock-up (KSU-767) used in

experimental studies by Kansas State University (KSU) [4], as described in the next section.

As the role of turbulence characteristics has been recognized to be very important for the intended analysis [5] [6], initial investigations have focused on the ability of turbulence modeling to reproduce the large-scale circulations in the cabin. Best results were obtained employing a Reynolds-Average-Navier-Stokes (RANS) approach with a modified version of the Realizable  $k$ - $\epsilon$  model, as the use of Large-Eddy-Simulations (LES) has shown to be prohibitively costly, taking into account the need to incorporate the heat flux from the manikins and, subsequently, the contaminant flow phase using an Eulerian approach. Setup conditions were prescribed to closely simulate the experiments by KSU [4]. In a first stage, symmetry has been assumed across the cabin's longitudinal midplane; periodic boundary conditions were enabled in meshing, with an outlet pressure condition allowing reverse backflow; in addition, Boussinesq's hypothesis was imposed. It is expected that the present simulations may provide solid guidelines regarding a foreseen future installation of bioaerosol sensors in each seat row during flight, thereby allowing an early warning about possible infected passengers and, ultimately, contributing to improve the control of various respiratory pathogens spread by air travel.

### 1.1 State-of-the-art

Due to COVID pandemic, there have been recent studies addressing this topic. Aiming to determine exposure risk, using optical sensors and collection techniques, dispersion and deposition of tracer aerosols was tested in the airframes of Boeing 767 and 777, on ground and in flight conditions, with gaspers active on ground [7], in a complementary investigation to a previous report [8]. These experimental results were compared in a computational study for a Boeing 737 where a manikin coughed polydisperse aerosols [9]. Both studies came to the conclusion that there is a low exposure risk.

In order to be able to compare data with the airframe testing, there is a need to accurately model the airflow. The KSU mock-up cabin can be used to directly compare because it has real salvaged parts of the diffuser from Boeing 767. Beneke [10] studied small diameter particle dispersion of talcum showing that regions close to the source had a high level of exposure. In a similar experiment, Shehadi [11] investigated optimal particulate sensor locations in the cabin. On the other hand, Trupka [12] studied the impact of a beverage cart on contaminant dispersion. Anderson studied the effect of gaspers using tracer gas on the cabin and used a more advanced thermal manikin [13]. Ebrahimi employed Large Eddy Simulation (LES) to study the airflow and tracer gas on a generic cabin (KSU-GEN) and used RNG  $k$ - $\epsilon$  in the simulation of the 11-row cabin by adjusting turbulence parameters at the diffuser slot, modeled as a rectangular opening [14]. Later, using smoke visualization, Shehadi [15] proposed flow patterns inside the cabin that indicated three large vortices along the cabin, namely one in the aft section, one in the middle section and one at the forward section, and studied experimentally the airflow distribution and turbulence in the longitudinal direction [16] [17]. These asymmetrical trajectories of the flow in the cabin were further explored by Keshavarz [18] with an added supplementary fan. The ventilation effectiveness in a B737 mock-up and B767 was studied in [19] using tracer gas. Later on, an expedient passenger isolation system (ISOPass) was developed and found to be highly effective when deployed [20] [21]. Finally, Mahmoud [22] also studied experimentally aerosol dispersion using tracer gas in several situations, i.e. continuous injection point source, and a coughing manikin, both with ISOPass deployed and undeployed, in the B737 mockup, the B767 mockup and the same B767 mockup using a different ventilation system more alike to airbus cabins.

Only few computational studies modeled a more detailed diffuser. Lin et al. [23] [24] reported that RANS simulations significantly underpredicted the turbulence intensity, therefore, using LES and experimental results they tuned a modification to a RANS  $k-\epsilon$  model with the goal of increasing the accuracy of the RANS simulation. They demonstrated that the turbulent kinetic energy was approximately eight times larger in LES than using standard  $k-\epsilon$  modeling. Mazumdar [25] modeled the entire KSU-767 cabin with the RNG  $k-\epsilon$  approach and compared with experimental data; it was reported that the diffuser breaks the main jet from the tubes into smaller jets that are governed by the spacer buttons and wall connectors locations, however there was a negligible net longitudinal flow with strong local longitudinal flows.

## 1.2 Mock-up Cabins

There are several mock-up cabins available worldwide, organized in [Table 1](#) based on information previously published in the literature [26]. To accurately simulate the airflow, it is necessary to know every detail of the cabin mock-up, especially the geometry of the diffuser, i.e., the outer and inner geometry that the air must travel until it arrives to the cabin space. Therefore, it was chosen the cabin with most documented data, namely the 767 mockup cabin from Kansas State University (KSU-767). According to the literature, the researchers use salvaged diffusers from aircraft, with real aircraft seats. Furthermore, simulation data can also be compared with data from Illinois University and Technical University of Denmark, however, care must be taken because the volumetric airflow rate, thermal boundary conditions and air properties will not be precisely the same.

The KSU-767 cabin is composed of ducting, diffuser, storage bin and seats. Before the air arrives to the cabin it passes through a HVAC Air filter, blown to desiccant dehumidification wheels and then an air conditioning system composed of three loops, subsequently proceeding to an electric heater, and finally arriving to the cabin ductwork. The cabin is composed of 11 rows with seats following the layout of the economy section (2-3-2) of a Boeing 767-300 aircraft, with the mixed class configuration type A door (24 first class seats and 224 economy seats) [27] [28]. The seats in the mock-up are filled with manikins wrapped with electric wire to create a thermal output of 100W. For the contaminant study, the injector is made of a copper tube with 25.4 mm radius. Gaspers were installed in 2012 in rows 5, 6 and 7 [13]; they are kept at a pressure of 498.18 Pa providing a flow rate of 1.6 L/s when fully opened; each gasper centerline or Personal Air Outlet (PAO) is separated 3 in (76.2 mm) from each other. The air from the gasper is extracted from the main supply duct.

**CFD STUDY OF AIRBORNE PATHOGENS DISPERSION INSIDE AN AIRCRAFT CABIN**

Model	Institute		Resources
<b>Most Reported Studies</b>			
<b>Boeing 737</b>	Purdue University	PU-737	[29], [30], [31], [32]
	Tianjin University	TJ1-737	[33], [34], [35], [36]
	Tianjin University (2021)	TJ2-737	[37]
	Kansas State University	KSU-737	[38], [19]
<b>Boeing 767</b> <i>*Real diffusers</i>	<b>Illinois University *</b>	IU-767	[39]
	<b>Kansas State University *</b>	KSU-767	[13], [11], [40], [22], [10]
	Purdue University	PU-767	[41], [42]
	Dalian University of Technology	DUT-767	[43]
	<b>Technical University of Denmark *</b>	DTU-767	[44]
<b>Boeing 767 scaled</b>	Purdue University	PU-767s	[26],[25]
<b>Boeing 777</b>	Syracuse University	SU-777	[45]
<b>Boeing 747</b>	Aircraft Environment Research Facility in CAMI	AERF-747	[46]
<b>Airbus 310</b>	FTF at Fraunhofer Institute	FTF-310	[47], [48], [49]
<b>Airbus 320</b>	German Aerospace Center (DLR)	DLR-320	[50], [51]
	Chongqing University	CU-320	[52], [53], [53]
<b>Airbus 380</b>	German Aerospace Center (DLR)	DLR-380	[54]
<b>A380 section</b>	German Aerospace Center (DLR)	DLR-380s	[55], [56]
<b>MD-82</b>	Tianjin University	TJ-MD82	[57], [58], [59], [60]
<b>Half Generic</b>	Kansas State University	KSU-GEN	[61], [14], [62], [63], [23]
<b>Other installations (new or owned by manufacturer)</b>			
<b>Generic</b>	Flexible Cabin Laboratory at CATR	FCL-CATR	[64]
<b>Boeing 737</b>	Fuselage Laboratory at CATR	FL-CATR	[64]
<b>Boeing 787</b>	Boeing Company at AIC	AIC-B787	[65]
<b>Airbus 340</b>	Airbus Company	A340	[26], [66]
<b>AIC – Aircraft Integration Center. FTF – flight test facility. CAMI – Civil Aerospace Medical Institute</b>			

Table 1 - Mock-up cabins available worldwide.

## 2. Methods

### 2.1 3D Modeling

Aiming to accurately model the KSU-767 cabin, extensive analysis of the documentation by KSU authors were analyzed [11] [22]. To aide future research on this topic, the files of the 3D models will be made available. Extensive details and drawings of the geometry used in this study can be found in [67]. The reference frame is always the same, on the figures a cube with the axes is indicative of the view at that figure.

The diffuser slot gap, i.e., the area between the edge of the radius of the stowage bin and the tip of the diffuser at the ceiling, is assumed to be the sum of the radius of the storage bin 0.75 in with the gap between the tip of diffuser and the end of the storage bin 0.5 in, summing to 1.25 in (31.75 mm). The spacing from the cabin centerline to the diffusers tip is 6.625 in (168.275 mm). The rest of the dimensions of the frontal area of the diffuser were extrapolated from available images and conjugated with available dimensions, however the image was not taken normal to the face. The thickness of the diffuser metal sheets was assumed to range from 1.016 to 2.032 mm, and the angle between the sheet and the ceiling 66.8 °. The distance between the center of the circular hose and the storage bin is 1.5 in (38.1) mm. The total number of outlets was assumed to be 30, with 596.9 x 177.8 mm (width x height) and a spacing of 39.0525 mm (from the walls) as well as a pitch of 635.9525 mm. The width of the center seats is assumed to be 62 in (1.5748m). Details about gaspers are mentioned on 3.2.2.

## 2.2 Computational Methods

The computational study was divided into different stages to accomplish the goal of the present investigation. In the first stage, the computational domain was defined as half the row 6 and used to verify the performance of turbulence models as well as to define parameters to build a good quality mesh. In the second stage, the computational domain was set as the west portion of rows 5,6 and 7. In the third stage, the computational domain was redefined as the west and east portion of rows 5,6 and 7. Finally, in the fourth stage, gaspers were added to the domain. This study will only focus on steady state conditions. In the second and third stages, the turbulence model was chosen to be the modified  $k-\varepsilon$  approach, and the Eulerian transport of species was used to simulate a continuous injection of a mixture of He and CO<sub>2</sub> in steady state conditions with moist air. In the fourth stage, gaspers were added at every row with moist air, and the flow conditions at the inlet nozzle were updated to account for the loss of volumetric flow rate. For the 2<sup>nd</sup>, 3<sup>rd</sup> and 4<sup>th</sup> stages, the applied turbulence model was the RANS modified realizable  $k-\varepsilon$  (rk $\varepsilon$ -mod).

### 2.2.1 Computational Domain

To build the 3D model of the cabin, Solidworks 2020 was used and then converted to Parasolid format. To extrapolate distances from pictures Geogebra and Adobe Photoshop were used. To extrapolate data from graphs WebPlotDigitizer 4.5 was used. To handle simple calculations Microsoft Excel was used. To clean the geometry of the 3D model and define the surfaces to be boundary conditions Ansys Spaceclaim 2021 was used. To handle the meshing, Ansys Fluent 2021 R1 [68] Meshing Watertight workspace was used. To perform the simulations, Ansys Fluent 2021 R1 was used. Care was taken because Spaceclaim was not directly used to model the geometry and conversion errors could occur and result in small faces or bad edges; for example, the buttons had to be redone.

The cabin geometry includes the internal parts of the diffusers (spacer buttons, connectors, joint spacers) which account for many walls and small features in small portion of the domain. This creates difficulties in creating a good quality mesh, possibly enhancing wall effects from the turbulence models. However, this is necessary to accurately model the flow that passes through the slot.

The longitudinal length of the full cabin of 11 rows is the same as the length of the west diffuser section 377.1 in (9.57834 m). The maximum transversal length of the cabin is 186 in (4.7244 m) and the height of the diffuser tip is 1.9812 m, while the maximum height is 82.5 in (2.0955 m). When choosing the geometry to simulate, only the seats and manikins from the desired row are kept. The manikins are modeled as simple box shaped based on previous literature [37]. Gaspers were modeled as simple cylinders directed normal to the surface they were in; the diameter and velocity were computed using relations from the literature [31].

The reference frame of the domain was the same as referenced in KSU documents. The origin is at the intersection between the cabin floor, the symmetry plane and the south wall, making z positive from south wall to north wall, y positive from the floor to the ceiling, and x positive when it is at the west portion and negative when is at east portion.

The figures presented below are to scale (separately from each other). In Figure 1 with half of the 6<sup>th</sup> row, the dimensions of the outlet are slightly different from the dimensions used afterwards. The geometry was extracted using the extracting volume tool from Spaceclaim. To avoid generation of mesh failure, a CAD correction was made: the spacing buttons were extruded until the next metal sheet, the manikins shoulder area was pulled to avoid merging the face with the seats. For the final simulations the geometry is shown in Figure 2.

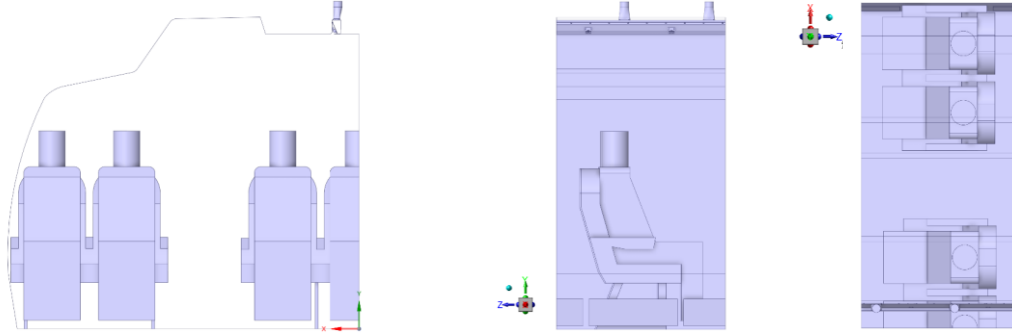


Figure 1 – 3D model of the extracted volume of half 6<sup>th</sup> row.

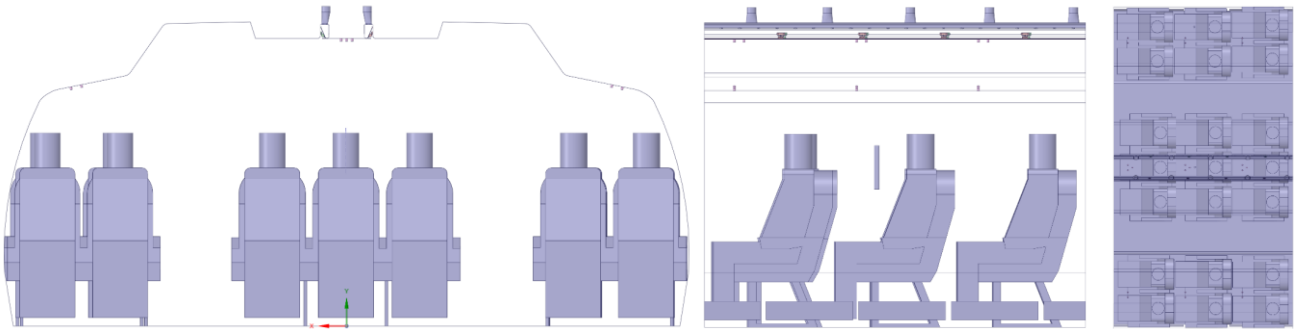


Figure 2 – 3D model of the extracted volume of rows 5, 6 and 7 with gaspers and injectors.

### 2.2.2 Turbulence Modeling

In previous work [23] [25] this kind of geometry was simulated using a modified  $k$ - $\epsilon$  model and a standard RNG  $k$ - $\epsilon$  model employing standard wall functions. The Finite Volume Method is used for the discretization of the flow equations. The Reynolds Averaging of the Navier Stokes (RANS) equations can be found in Fluent's manual [68].

The chosen turbulence model is a modified version of the realizable  $k$ - $\epsilon$  model, by changing the source term  $S_k$  in the turbulent kinetic energy  $k$ -equation and changing the turbulent Prandtl number for the turbulent dissipation rate  $\sigma_\epsilon$ , based on findings from the literature [23]. Equations (1) and (2) presented here are the original realizable  $k$ - $\epsilon$  model implemented in Fluent for the transport of turbulent kinetic energy ( $k$ ), and its dissipation rate ( $\epsilon$ ) respectively.

$$\frac{\partial}{\partial t}(\rho k) + \frac{\partial}{\partial x_j}(\rho k u_j) = \frac{\partial}{\partial x_j} \left[ \left( \mu + \frac{\mu_t}{\sigma_k} \right) \frac{\partial k}{\partial x_j} \right] + G_k + G_b - Y_M + S_k - \rho \epsilon \quad (1)$$

$$\frac{\partial}{\partial t}(\rho \epsilon) + \frac{\partial}{\partial x_j}(\rho \epsilon u_j) = \frac{\partial}{\partial x_j} \left[ \left( \mu + \frac{\mu_t}{\sigma_\epsilon} \right) \frac{\partial \epsilon}{\partial x_j} \right] + C_{1\epsilon} \frac{\epsilon}{k} (C_{3\epsilon} G_b) - C_2 \rho \frac{\epsilon^2}{k + \sqrt{\nu \epsilon}} + S_\epsilon + \rho C_{1S} \epsilon \quad (2)$$

The default constants are  $C_{1\varepsilon} = 1.44$ ;  $C_2 = 1.9$ ,  $\sigma_k = 1.0$ ,  $\sigma_\varepsilon = 1.0$ . In the realizable model,  $C_\mu$  is a function of the mean strain  $S$  and rotation rates  $\tilde{\Omega}_{ij}$ , angular velocity of system rotation and turbulence fields  $k$  and  $\varepsilon$ .  $C_\mu$  recovers standard value of 0.09 for an inertial sublayer in an equilibrium boundary layer. The option to include the rotational term  $-2\varepsilon_{ijk}\omega_k$  was enabled due to the use of a sliding mesh and multiple reference frames not being used in this study.

To implement the turbulence model modification, source terms of the  $k$ -equation used in Fluent were compared with the one used in the literature to integrate the previous applied constant in [23]  $C_{k2} = 0.77$ , a new constant had to be created  $C_{k3} = 1 - 0.77 = 0.23$  and integrated in the User Defined Function (UDF) (see Appendix Source Term UDF), as shown in equation (3). The term  $(S_k - \rho\varepsilon)$  is from equation (1) while the term  $(C_{k2}\rho\varepsilon)$  arises from the  $k$ -equation in [23].

$$\begin{cases} S_k = C_{k3}\rho\varepsilon \\ S_k - \rho\varepsilon = C_{k2}\rho\varepsilon \end{cases} \rightarrow C_{k3}\rho\varepsilon = (1 - C_{k2})\rho\varepsilon = 0.23\rho\varepsilon \quad (3)$$

The turbulent Prandtl number for the turbulent dissipation rate was directly implemented in the dialog box as  $\sigma_\varepsilon = 1.67$ .

Near-wall modeling was handled with Menter-Lechner functions to provide  $y^+$  insensitive wall treatment and avoid drawbacks from using the turbulent Reynolds number for selecting the flow regime such as: treating low  $k$  regions with near-wall formulas despite being far away from the wall and problems with convergence in coarse regions. This near-wall treatment is based on the idea of adding a source term in  $k$ -equation to account for near-wall effects which will be active only in the viscous sublayer, and also accounting for low-Reynolds number effects.

### 2.2.3 Contaminants Modeling

For the species transport, Diffusion Energy Source and Thermal diffusion options were enabled. Nitrogen was defined as the last species.

## 2.3 Materials and operating conditions

When the flow was simulated without species, the material that was considered was moist air. When species were turned on, there were 6 different species: nitrogen  $N_2$ , oxygen  $O_2$ , water vapor  $H_2O$ , argon  $Ar$ , carbon dioxide  $CO_2$  and helium  $He$ . In Fluent, the materials were defined as followed in Table 2.

	Single Phase	Mixture	Species
<b>Material</b>	Dry air	Moist air	$N_2, O_2, H_2O, Ar, CO_2, He$
<b>Density</b>	Ideal gas	Ideal-gas	-
<b>Specific Heat Capacity</b>	Constant = $1006.13 \text{ J}\cdot\text{kg}^{-1}\cdot\text{K}^{-1}$	Mixing Law	Constant
<b>Thermal Conductivity</b>	Polynomial	Ideal gas mixing law	Kinetic theory
<b>Viscosity</b>	Sutherland	Ideal gas mixing law	Sutherland
<b>Molecular Weight</b>	Constant = $28.96495 \text{ g/mol}$	-	Constant
<b>Mass Diffusivity</b>	-	Kinetic Theory	-
<b>Thermal Diffusion Coefficient</b>	-	Kinetic Theory	-

Table 2 – Materials definition.

The operating conditions are the same for every simulation. The Boussinesq temperature was chosen to be  $21^\circ\text{C}$  because at steady state conditions the average temperature is known to be between  $21^\circ\text{C}$  and  $22.5^\circ\text{C}$ . The operating pressure was the same as inside the mock-up, set to  $98882.53193 \text{ Pa}$ , and

the local gravity acceleration evaluated at Seaton Hall in (latitude, longitude, mean sea level height) = (39.18916,-96.58260,1070 ft) [69] resulting in  $-9.79958 \text{ m/s}^2$  on the  $y$ -direction [70].

## 2.4 Solution Methods

For the single-phase simulations, the coupled method with default pseudo transient explicit relaxation factors was used for the pressure-velocity coupling and changed to the Semi-Implicit Method for Pressure Linked Equations-Consistent (SIMPLEC) when species transport was activated. The discretization of pressure was used with the Pressure Staggering Option (PRESTO!). The summary of applied methods can be seen in the Table 3.

	Single Phase	Species transport
<b>Pressure-Velocity</b>	Coupled	SIMPLEC, skewness correction =2
<b>Spatial Discretization</b>		
<b>Gradient</b>	Least Squares Cell Based	Least Squares Cell Based
<b>Pressure</b>	PRESTO!	PRESTO!
<b>Density, momentum, turbulent kinetic energy, turbulent dissipation rate, species, energy</b>	Second Order Upwind	Second Order Upwind
<b>Additional</b>	Warped-Face gradient correction, High order term relaxation factor of 0.25 all variables For the Coupled method - Pseudo transient, time factor = 1	

Table 3- Chosen methods for pressure-velocity coupling and discretization.

To start the solution, hybrid initialization was employed. Then for the diffuser region ( $y > 1.9812 \text{ m}$ ) temperature was set to  $15.6 \text{ }^\circ\text{C}$  and  $21 \text{ }^\circ\text{C}$  for everywhere else to speed up convergence. When species were modeled, the domain was patched with the same molar fraction as the inlets. Residuals were also monitored. For the single-phase, continuity residuals were kept below  $1 \times 10^{-2}$ , for velocities under  $1 \times 10^{-5}$ , for turbulent kinetic energy and dissipation rate under  $1 \times 10^{-5}$ , and for energy under  $1 \times 10^{-7}$ . For the species simulation, residuals of He and  $\text{CO}_2$  were kept below  $1 \times 10^{-5}$ , and for Ar,  $\text{H}_2\text{O}$  and  $\text{O}_2$  below  $1 \times 10^{-7}$ . To ensure convergence, multiple physical quantities were monitored, as presented in Table 4.

### Monitor quantities

<i>Turbulent kinetic energy</i>	inlets, slot, outlets, XY-plane of row 6, XZ-plane of breathing area at $y = 1.25\text{m}$
<i>Temperatures</i>	Volume average temperature of all domain, floor, slot, manikins, z-plane row 6, XZ-plane of breathing area
<i>Turbulence intensity</i>	Slots, inlets, outlets, XY-plane of row 5,6,7 and y-plane of breathing area
<i>Massflow rate</i>	Inlets, slots, outlets, periodic faces, XY-planes of rows 5,6,7 and XZ-plane of breathing area
<i>CO<sub>2</sub> molar fraction (when species were active)</i>	Monitored at different points to match experimental results; surface average in inlet, exit and volume average of domain

Table 4- Monitored physical quantities

## 2.5 Mesh Generation

The mesh was composed of prism layers and polyhedral elements. Special care was taken in the region of  $1 < y^+ < 5$ , so a local face size was chosen near the small parts of the diffuser (0.2 mm in the buttons). The surface mesh was set to have a minimum of 0.5 mm and maximum of 50 mm. The generated volume mesh had 2.51 million elements with a minimum orthogonal quality of 0.122 and a maximum aspect ratio of 508. The high aspect ratio cells are formed on the areas with a high face size and a small prism layer height. This was a compromise to not increase more the number of elements.



It is noted that the diffuser region ( $y > 1.9812$  m), i.e., above the slot, contains 89% of the total number of cells. The mesh domain for the half of the 6<sup>th</sup> row is between  $4.17114$  m  $< z < 5.305198$  m,  $0 < y < 2.201037$  m and  $0 < x < 2.362186$  m. The final volume mesh for the half 6<sup>th</sup> row can be seen in Figure 3.

A mesh with similar parameters was generated for the 3 rows with injectors and gaspers. Smaller local face sizes were defined at the injector and gasper faces when the domain simulated changed. The domain for 3 rows with both sides without gaspers contained 5.78M elements, and with gaspers it was formed by 6.51M elements. The longitudinal domain without gaspers was  $3.43285$  m  $< z < 6.049770$  m and with gaspers  $3.432836$  m  $< z < 6.049788$  m. Near the slot area the mesh is more refined and the details of the internal parts are depicted in Figure 4. The resulting wall  $y^+$  is shown in Figure 5.

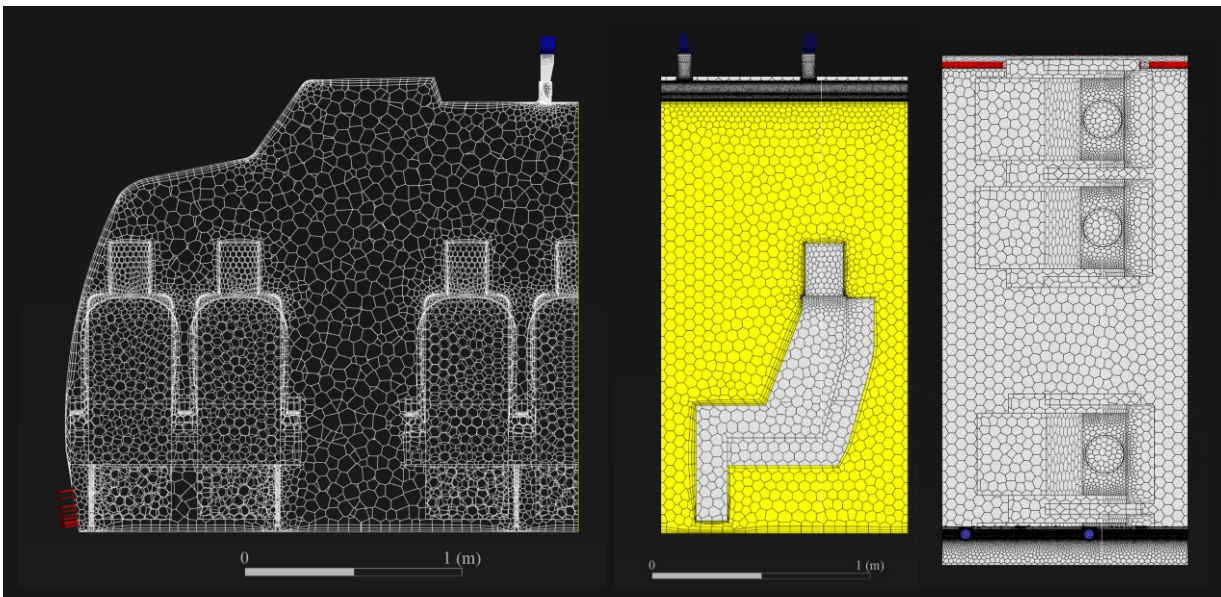


Figure 3 – Volume mesh for the west portion of the 6<sup>th</sup> row.

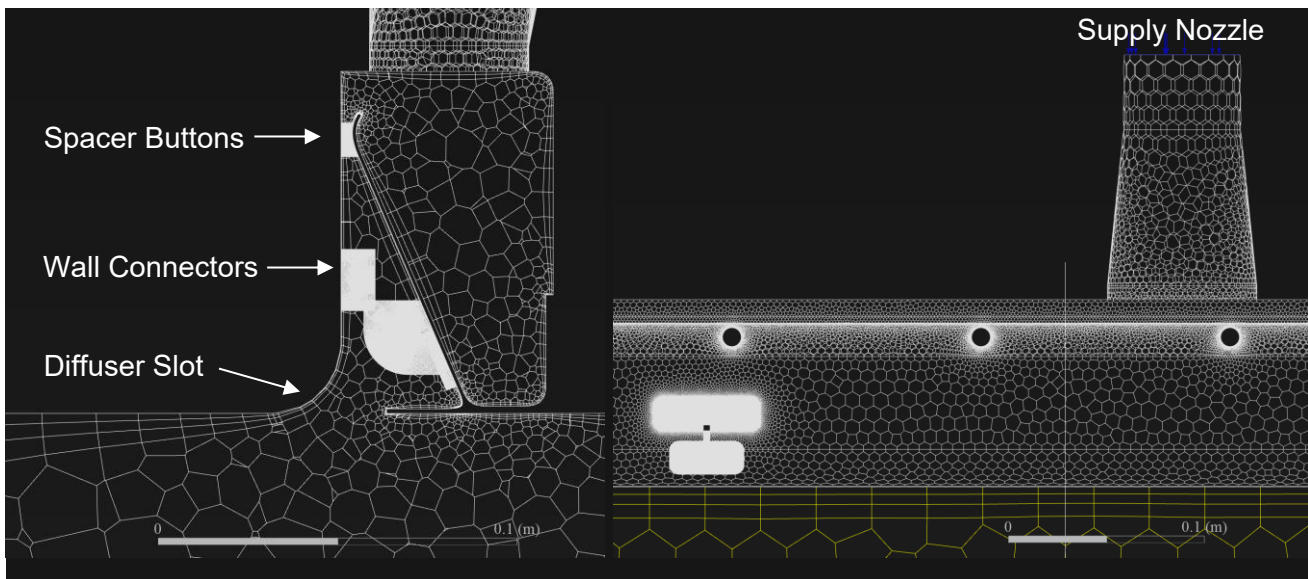


Figure 4 – Zoom-in of the mesh near the diffuser slot.

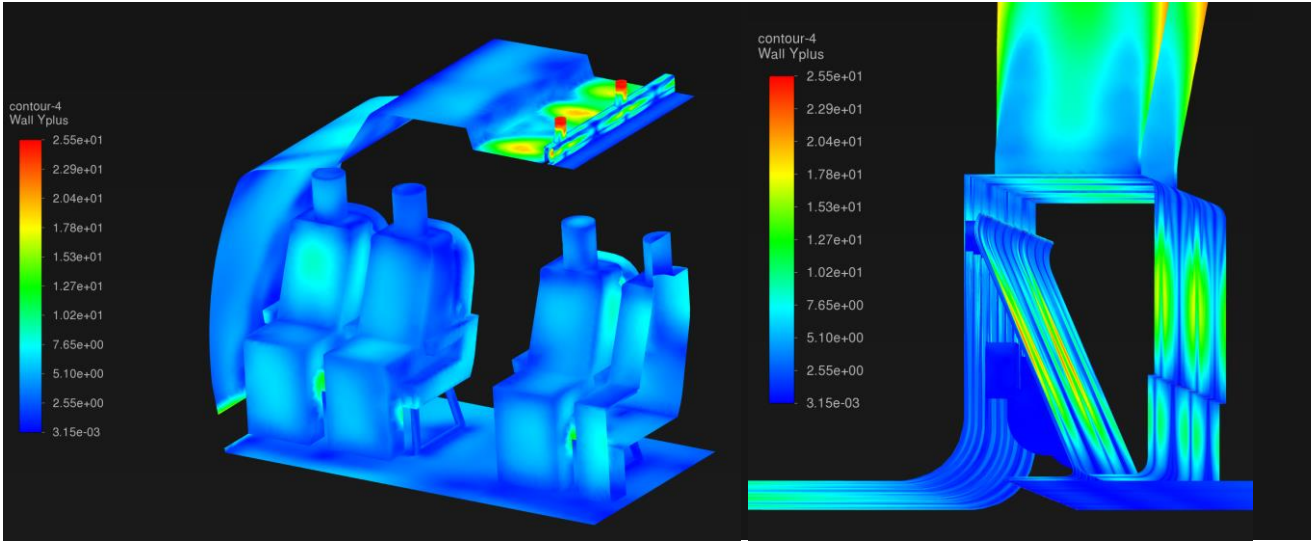


Figure 5 – Wall  $y^+$  of the west portion of 6<sup>th</sup> row

## 2.6 Boundary Conditions

As mentioned earlier, our goal was to simulate the same conditions as those in the mock-up of KSU. The inlets were the supply nozzles that feed the diffuser, with a diameter of 60.325 mm, with a flow rate of 1400 CFM (660.73 L/s) distributed through 34 nozzles. This defines an average inlet velocity to be 6.799 m/s and at a static temperature of 15.6 °C. The outlets were allowed to have reverse flow and prescribed at a temperature of 22°C. To better simulate the physical behavior of the flow, translational periodic boundary conditions were defined at the front and back faces of the domain with flow defined for the z axis, with a pressure gradient of 0 Pa/m and 21°C for the backflow. When just the west portion of the domain was simulated, a symmetry condition was applied to the plane  $x = 0$ . The temperature of the manikins is not referred in the literature, so the output of 100W was divided by the manikin surface area which resulted in a heat flux of 52.82 W/m<sup>2</sup>.

When gaspers were added, the flow rate directed to the supply nozzles was adjusted. There are 21 gaspers, totaling 33.6 L/s, thus, 627.13 L/s are directed to the 34 nozzles giving an average inlet velocity of 6.453 m/s. Geometrically, the gaspers were assumed to be the same as in [31], therefore the same empirical relations could be used to determine the equivalent cylinder diameter (4) and average velocity (5).

$$d = \frac{4QB}{\pi B^*} \quad (4)$$

$$U_{m,0} = \frac{\pi}{4Q} \left( \frac{B^*}{B} \right)^2 \quad (5)$$

By considering  $B = 6.2$ ,  $B^* = 0.75$  and applying the volumetric flow rate  $Q = 1.6$  L/s used in KSU, the equivalent diameter  $d$  results 16.84mm, and the average velocity at the circular face  $U_{m,0}$  is 7.183 m/s.

Physically there is just one injector at the simulated cabin domain, therefore, after convergence, the profiles of velocity, temperature, turbulent kinetic energy and turbulent dissipation rate were extracted and applied at the front and back faces. This way, it was possible to specify the species molar fraction

to be the same as the supply nozzle. In the case of gaspers, a trade-off was taken to not simulate more rows, as this would be true for an infinite number of rows; however, the mock-up in KSU has only gaspers at rows 5, 6 and 7.

When the species were simulated, the molar fractions of moist air with a relative humidity (RH) assumed to be 15% were prescribed at the inlets of the supply nozzles. The supply air CO<sub>2</sub>-concentration read by instruments was 400 ppm, so the applied molar fraction ( $X_i$ ) at the inlets of CO<sub>2</sub> was set to 400 ppm as well. ( $X_{CO_2,moist\ air} = 0.04\%$ ). The injector of the contaminant was a mixture of CO<sub>2</sub> ( $Q_{CO_2} = 5L/min$ ) and He ( $Q_{He}=3.07L/min$ ). Assuming that both tanks of CO<sub>2</sub> and He were at the same temperature and pressure, as well that the exit pressure of the tube and the pressure where they were measured is the same as the cabin, by applying mass and energy balance their properties can be calculated. The injector speed had an average velocity of 0.2654 m/s and a temperature of 15.6 °C. For reference, the universal gas constant used was  $R_u = 8.314472\ J/(kg\cdot K)$ .

The molar fraction of water was computed using the definition of RH and the Buck equation for the saturated water vapor pressure. This resulted in 0.26883% of H<sub>2</sub>O and 99.73117% of dry air. Dry air molar fractions of O<sub>2</sub>, Ar and He were extracted from International Civil Aviation Organization (ICAO) standard atmosphere manual [71]. Using ideal gas mixtures properties and relations [72] the molar fractions of each component were obtained. The viscosity was computed using Sutherland and Wilke's formula [73]. Table 5 shows the computed properties.

Properties	Moist air	Contaminant
$X_{N_2}$	$7.7869466 \times 10^{-1}$	0
$X_{O_2}$	$2.0889691 \times 10^{-1}$	0
$X_{H_2O}$	$2.6883154 \times 10^{-3}$	0
$X_{Ar}$	$9.3148911 \times 10^{-3}$	0
$X_{He}$	$5.2259132 \times 10^{-6}$	0.38042131
$X_{CO_2}$	$4.0000000 \times 10^{-4}$	0.61957869
<b>Mean Molecular Weight</b>	28.9365 g/mol	28.7903 g/mol
<b>Dynamic Viscosity</b>	$1.795725 \times 10^{-5}\ Pa \cdot s$	$1.576753 \times 10^{-5}\ Pa \cdot s$
<b>Density</b>	$1.191817888\ kg/m^3$	$1.185793652\ kg/m^3$

Table 5 – Species properties.

As for the turbulence parameters, the turbulent intensity ( $TI$ ) was calculated using equation (6) for fully developed duct flow and the Reynolds number was computed using the diameter [74]. In addition, Table 6 shows a summary of the boundary conditions used in the present study.

$$TI = 0.16 Re_{Dh}^{-1/8} \quad (6)$$

$$Re_{Dh} = \frac{\rho U D_h}{\mu} \quad (7)$$

$$TI = \frac{1}{|U|} \sqrt{\frac{2}{3}k} \quad (8)$$

	Momentum and Energy	Species Activated	
<b>Supply Nozzle Velocity</b>	$\vec{u} = -6.79921 \vec{e}_y \text{ m/s}$ $D_h = 0.060325 \text{ m}, TI = 4.463\%, T = 15.6^\circ\text{C}$	$X_{N_2}$	$7.7869466 \times 10^{-1}$
		$X_{O_2}$	$2.0889691 \times 10^{-1}$
		$X_{H_2O}$	$2.6883154 \times 10^{-3}$
	With gaspers $\vec{u} = -6.45345 \vec{e}_y \text{ m/s}$ $D_h = 0.060325 \text{ m}, TI = 4.492\%, T = 15.6^\circ\text{C}$	$X_{Ar}$	$9.3148911 \times 10^{-3}$
		$X_{CO_2}$	$4.0000000 \times 10^{-4}$
<b>Outlets</b>	Pressure outlet, backflow $T = 22^\circ\text{C}$	Same as supply nozzle	
<b>Manikins Walls</b>	Heat flux = $52.818 \text{ W/m}^2$	Zero flux	
<b>Front and back faces</b>	Translational PBC, $dp/dz = 0 \text{ Pa/m}, T = 22^\circ\text{C},$ flow direction z	Profiles fixed, species same as supply nozzle	
<b>Injector</b>	$\vec{u} = 0.2654 \vec{e}_y \text{ m/s}$ $D_h = 0.0254 \text{ m}, TI = 5\%, T = 15.6^\circ\text{C}$	$X_{He}$	0.38042131
		$X_{CO_2}$	0.61957869
<b>Other Walls</b>	Adiabatic	Zero Flux	
<b>Gaspers</b>	$ \vec{u}  = 7.183053 \text{ m/s}$ $D_h = 0.016840715 \text{ m},$ $TI = 5.195\%, T = 15.6^\circ\text{C}$	Same as supply nozzle	

Table 6 – Summary of boundary conditions.

### 3. Results and Discussion

#### 3.1 Half-row Single-phase Simulation

During the first stage of the numerical simulations, several categories of turbulence models were experimented. In summary, turbulence models employing the  $k-\epsilon$  approach performed the best overall,  $k-\omega$  and SST models performed poorly in the region past the slot. The 3-equation model  $k-kL-\omega$  performed qualitatively well, however, when checked in quantitative comparisons with experimental results from the probe it exhibited spikes of velocity without physical meaning.

Before applying the modification to the turbulence model, it was noticed that this modification was computed in isothermal conditions for a supply nozzle flow rate about 60% of the flow rate set in KSU-767 supply nozzle ( $0.6Q_{KSU} = 11.2 \text{ L/s}$ ,  $Q_{KSU} = 19.4 \text{ L/s}$ ). Therefore, a validation of the turbulence model was needed to advance to the next phase. To accomplish this important task, the contours of velocity were compared with for different conditions: isothermal flow with 60% of the flow rate, non-isothermal flow with 60% of the flow rate, and non-isothermal flow with 100% of the flow rate.

In Figure 6 ( $z = 4.9\text{m}$ ) the Coanda effect at the non-isothermal condition [75] was clearly decreased by the thermal plumes from the manikins which resulted in directing the jet more to the center of the side passengers. Hence, the flow was divided into two main vortices in the transversal plane ( $XY$ -plane). This is due to strong buoyancy effects from the thermal plumes of the manikins. The isothermal results were consistent with Lin 2005 [23].

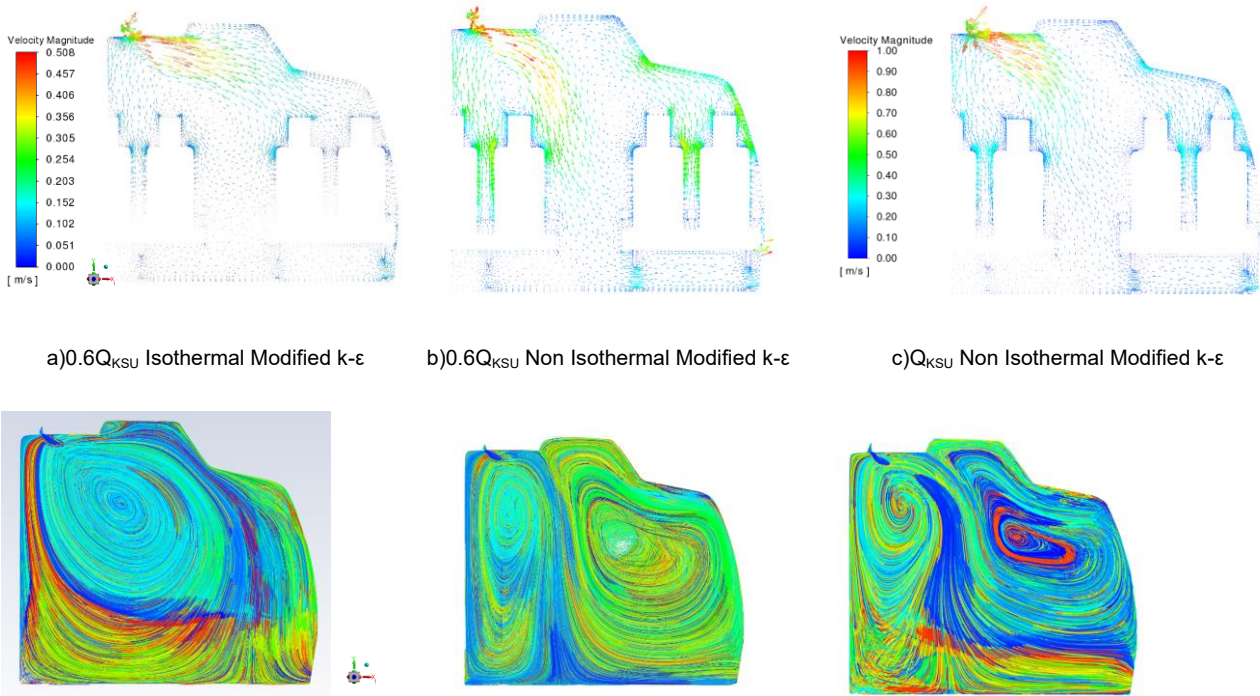


Figure 6 – Impact of flow rate and temperature on the cabin velocity field and pathlines

It is well known that  $k-\epsilon$  models are dissipative and the present modification allowed to decrease the dissipation. So, the surface averaged turbulent kinetic energy at the slot area was monitored. It was found that for the realizable  $k-\epsilon$  non-modified model  $Tl_{slot} = 41\%$  and  $k_{slot} = 0.93 \text{ m}^2/\text{s}^2$ , while for the modified model,  $Tl_{slot} = 66\%$  and  $k_{slot} = 1.9 \text{ m}^2/\text{s}^2$ . As for the 3-equations transition model  $k-kL-\omega$ , it was found that the flow is highly transitional, and the total fluctuating kinetic energy at the slot area was  $k_{slot} = 3.8 \text{ m}^2/\text{s}^2$

Quantitative experimental data of velocity magnitude obtained by an omnidirectional TSI Inc. probe near the slot [40] was compared with results from the simulation. The exact location of the computational probe is set here at  $x = 0.225435\text{m}$ ,  $y = 1.968027 \text{ m}$  and  $4.171178 \text{ m} < z < 5.30515 \text{ m}$ . In Figure 7, the velocity from the computational probe with different turbulent models is overlaid with the experimental data, and the west diffuser geometry is scaled to the z-direction.

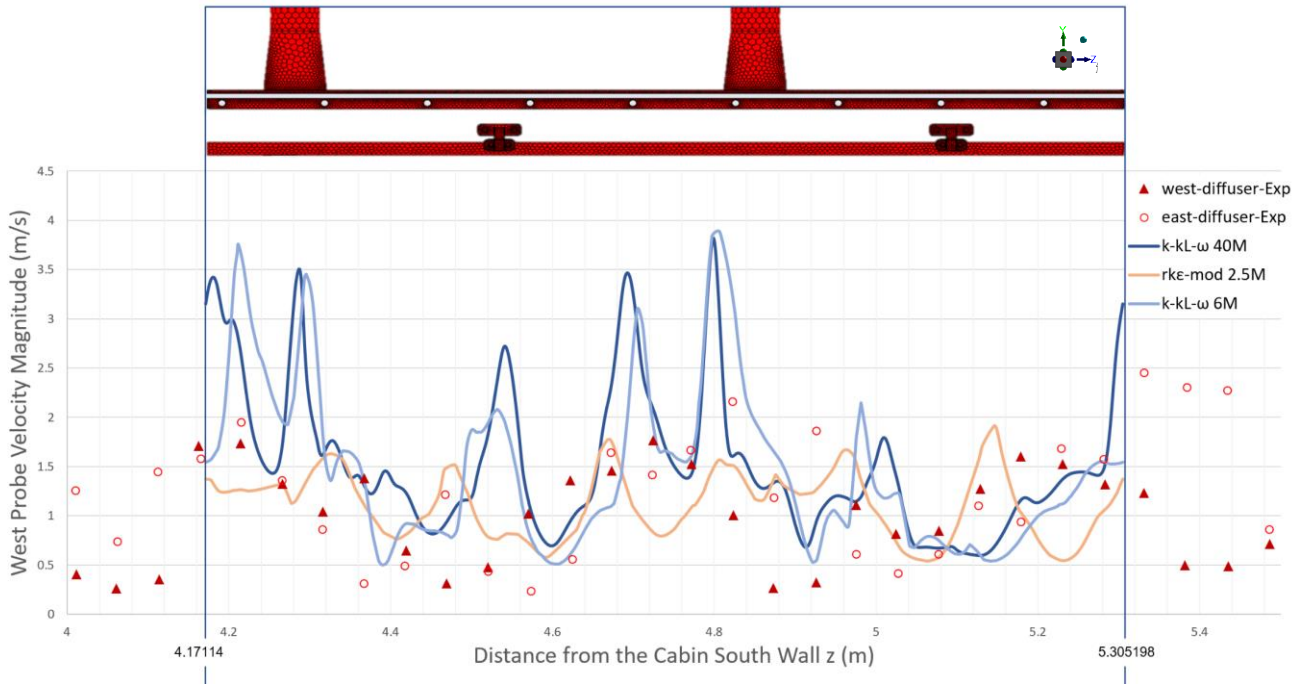


Figure 7 - Velocity magnitude at west probe for different turbulence models.

In the slot area, the flow was rather complex as reported in the literature. In Figure 8, one may observe the plots of turbulent kinetic energy, velocity magnitude, turbulence intensity and static temperature at the slot. In Figure 9 it can be seen a detailed area of the velocity magnitude from the diffuser jet. In Figure 10 it can be seen that the modification applied to the  $k-\epsilon$  model improved the accuracy of the simulation at these critical locations. The data in the plot of turbulence intensity is computed using equation (8).

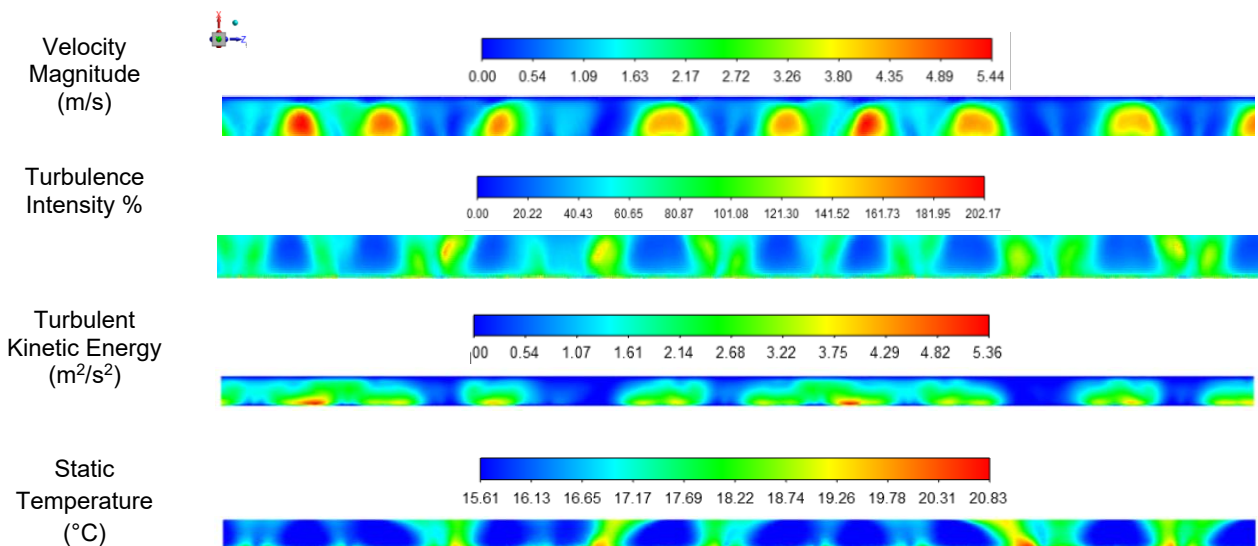


Figure 8 – Contours of flow quantities at the slot area.

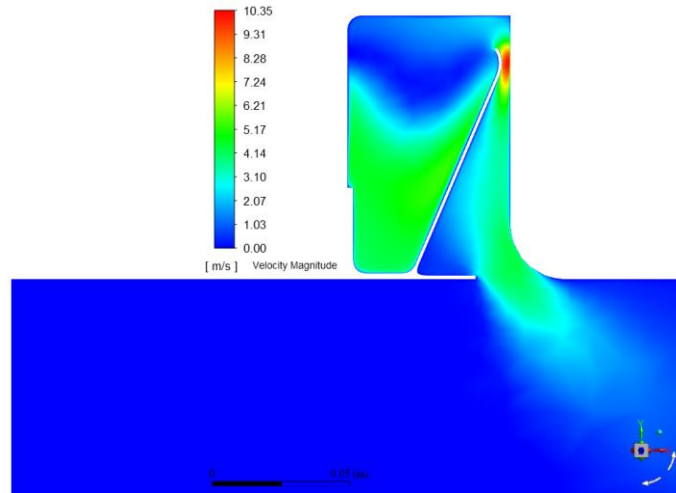


Figure 9 – Velocity magnitude contour for the diffuser at  $z = 4.783415$  m.

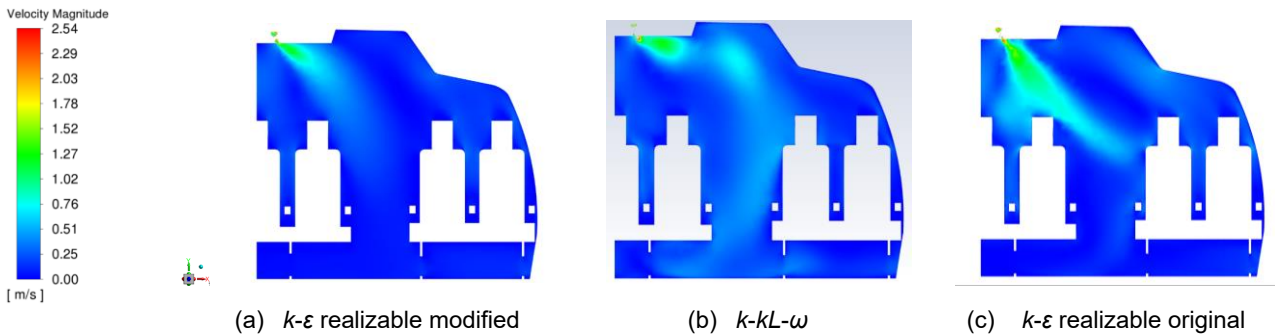


Figure 10 – Velocity magnitude contours for different turbulence models.

### 3.2 Three-rows Simulation

#### 3.2.1 Momentum and Energy

In Figure 11 it can be seen the results of the simulation from 3 rows when the injection at G6 was activated. Despite the geometrical asymmetry in the diffuser parts, i.e., the diffuser buttons, connectors and joints not being in the same plane and the seats not being on the same plane, the flow appears to be symmetric. It is noted that in this domain, the spacer joints were not simulated. The domain could be halved, however, to simulate the injection at the center of the cabin D6, the west and east portion needed both to be simulated.

As can be seen in Figure 11, there is a significant longitudinal velocity on the aisles area and the flow is governed by two large vortices in the transverse plane. In the symmetry plane, the influence of the thermal plume makes the velocities reach 38 cm/s. The injector has a velocity of 26 cm/s, however, globally this contaminant does not significantly disturb the flow, therefore one may assume that it behaves mostly as a passive contaminant.

Regarding the temperatures, when 3 rows are simulated with the injector turned on G6, the average temperature of the cabin is 22.3°C, while the average temperature of the manikins is 32.1°C. As with Figure 7, experimental data was compared with the computational probe for the west and east domain in Figure 12.

# CFD STUDY OF AIRBORNE PATHOGENS DISPERSION INSIDE AN AIRCRAFT CABIN

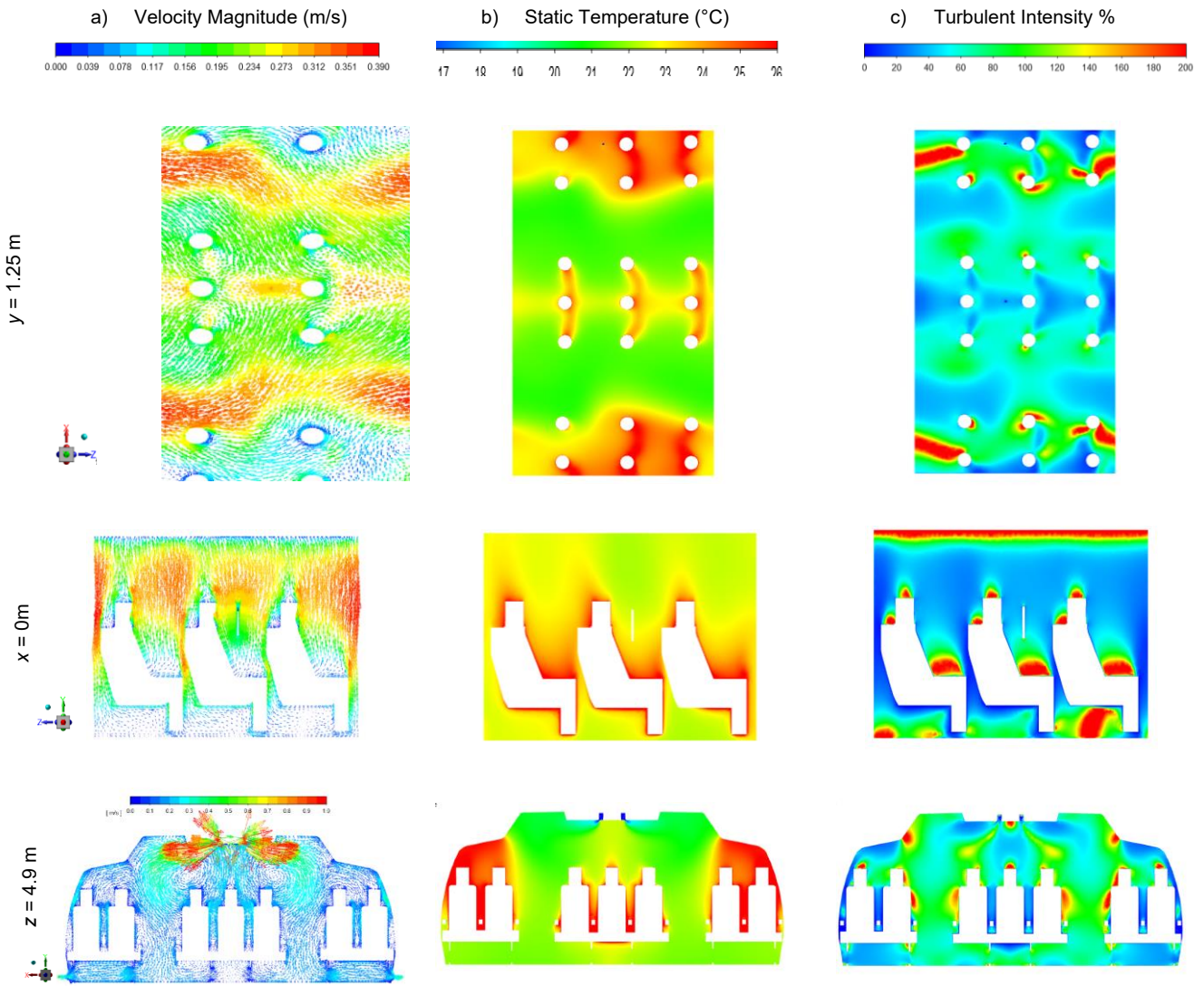


Figure 11 – Velocity, temperature, and turbulence intensity contours for 3 rows with G6 injector.

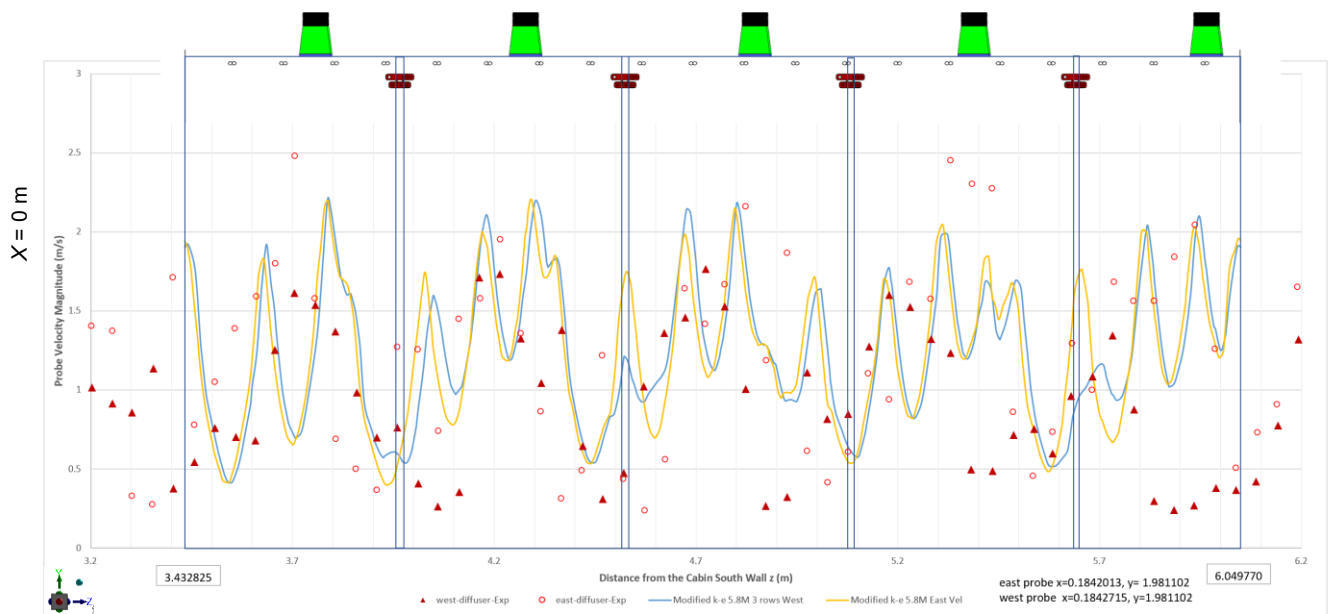


Figure 12 – Velocity magnitude at probes through 3 rows versus experimental data.



### 3.2.2 Contaminants

The full 11-row cabin interior with the origin of the reference frame and numbers of rows and letters of columns can be seen in Figure 14. Gaspers are considered to be 533 mm in front of the seat headrest, hence the gaspers on the 5<sup>th</sup> row are located at  $z = 3.63855$  m, on the 6<sup>th</sup> row at  $z = 4.47853$  m, and on the 7<sup>th</sup> row at  $z = 5.31343$  m [13]. The first gasper of the 2-cluster on rows F, G correspond to  $x = 1.82762$ m, and the second has  $x = 1.89938$ m

Figure 14 shows the results of the molar fraction of CO<sub>2</sub> in ppm overlapped with the experimental data from the literature [22]. The injector center face at D6 is at  $(x, y, z) = (0.005465$  m,  $1.250235$  m,  $4.621249$  m), while the injector center face at G6 is at  $(x, y, z) = (2.06414$  m,  $1.250234$  m,  $4.61185$  m). The distances of the points in the same line are 0.84 m between each other, and the experimental results are overlaid in the pictures. Discrepancies to the experimental results are noticeable. This difference can be explained by the absence of gaspers in the simulation which would create high momentum cold jets and decrease the momentum of the thermal plume as well as, depending on the direction of gaspers, redirect the trajectory of the contaminants.

Furthermore, one limitation of this simulation is to imply periodic boundary conditions which would create an infinite number of rows; however, the mock-up cabin is composed of only 11 rows. According to the image of the trajectory of the tracer gas suggested by Shehadi [15], this would create one large vortex near each end and two vortices near the center, probably caused by the influence of the physical cabin walls at the extremities. It is noted that it is not clear whether gaspers were turned on in Shehadi's study.

In Figure 13 and Figure 14 the molar fraction of CO<sub>2</sub> is plotted in the planes that cross the center of the respective injector. Figure 13 c) shows the YZ plane in the center of G6, Figure 13 d) portrays the YZ plane in the center of D6, Figure 13 a) depicts the XY plane in the center of G6, and Figure 13 b) illustrates the XY plane of D6. Moreover, Figure 14 a) and b) show the plane of breathing area corresponding to  $y = 1.25$  m (same as the injection).

With gaspers off, it can be seen that the thermal plumes transfer momentum to the convective transport of the contaminant CO<sub>2</sub>. When injected at the side wall, and because of the low ceiling, the contaminant is transported to row 7 eventually putting the passengers in risk. On other hand, when injected at D6, the contaminant climbs higher, which allows it to dissipate into the back rows, storage bins and aisles. Surprisingly, it appears that passengers seating next to the source D6 are not that much affected by the contaminant due to the thermal plumes and the large vortex that pushes the air away [76]. However, when injected at the side, there is significant transverse transport explained by the presence of a small vortex caused by the flow as seen in Figure 11 a).

CFD STUDY OF AIRBORNE PATHOGENS DISPERSION INSIDE AN AIRCRAFT CABIN

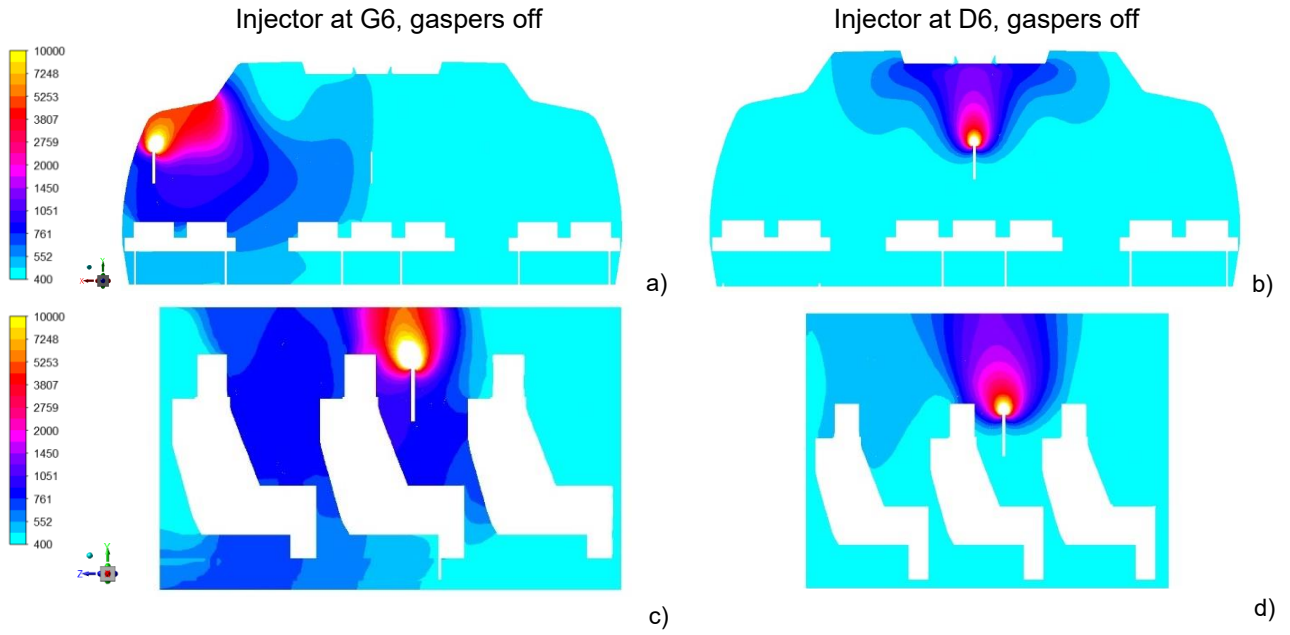


Figure 13 – Gaspers off: molar fraction of CO<sub>2</sub> in ppm at front and side planes.

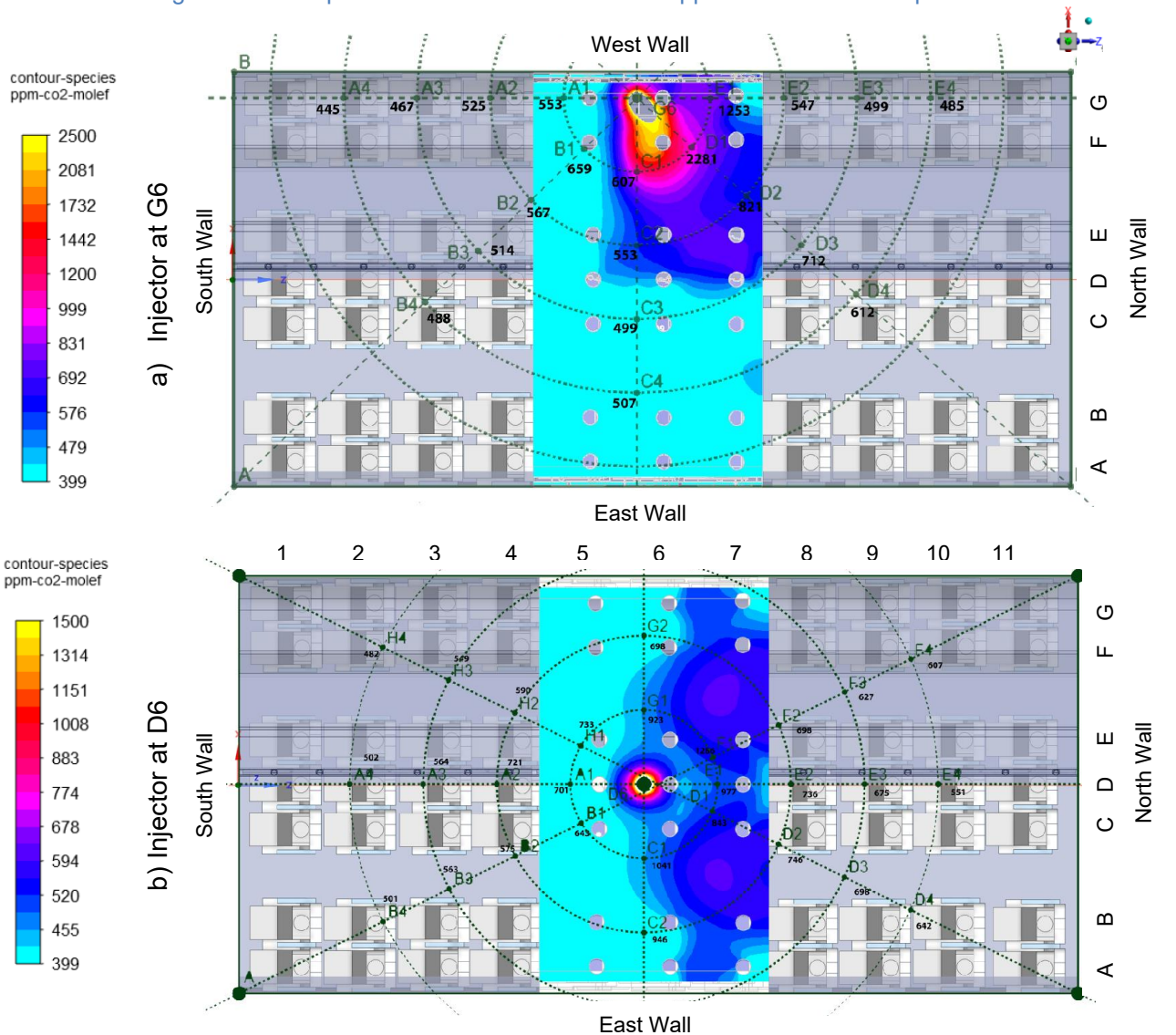


Figure 14 – Gaspers off: Comparison of CO<sub>2</sub> molar fractions at breathing area injected at a) side, and b) center.

### 3.3 Effect of Gaspers

The impact of gaspers on the continuous injection of the tracer gas was studied as well as the variation in velocity direction, using the same mesh (for each inclination), by adjusting the velocity components at the boundary conditions dialog box. The tested velocity inclinations were as follows: normal to the surface where the gaspers were in, at an inclination of  $45^\circ$  and  $60^\circ$  with the XZ plane. The gaspers were only tilted across the YZ plane, and this inclination can be observed in [Figure 16 d\)](#) and [e\)](#). Similar to the approach followed in the previous subsection, the molar fraction of  $\text{CO}_2$  was plotted at different planes. The side plane YZ is shown in [Figure 15 a\) b\), and c\)](#), together with [Figure 16 d\), e\) and f\)](#); the frontal plane XY is portrayed in [Figure 15 d\), e\), and f\)](#) together with [Figure 16 a\), b\), and c\)](#); the breathing area  $y = 1.25\text{m}$  plane is depicted in [Figure 17](#).

When the gasper was tilted, there was a significant amount of momentum added to the longitudinal direction which transported the contaminant to the back row, while the vertical velocity was not enough to overcome the buoyancy of the thermal plumes, thus allowing the contaminant to dissipate upwards but closer to the seating passengers. This can be desirable because of the counter-clockwise circulation that will act pushing the contaminant to the storage bin. However, when injected at the side of the cabin, the close proximity to the ceiling remains to be detrimental, thereby increasing the concentration of contaminant at the 7<sup>th</sup> row.

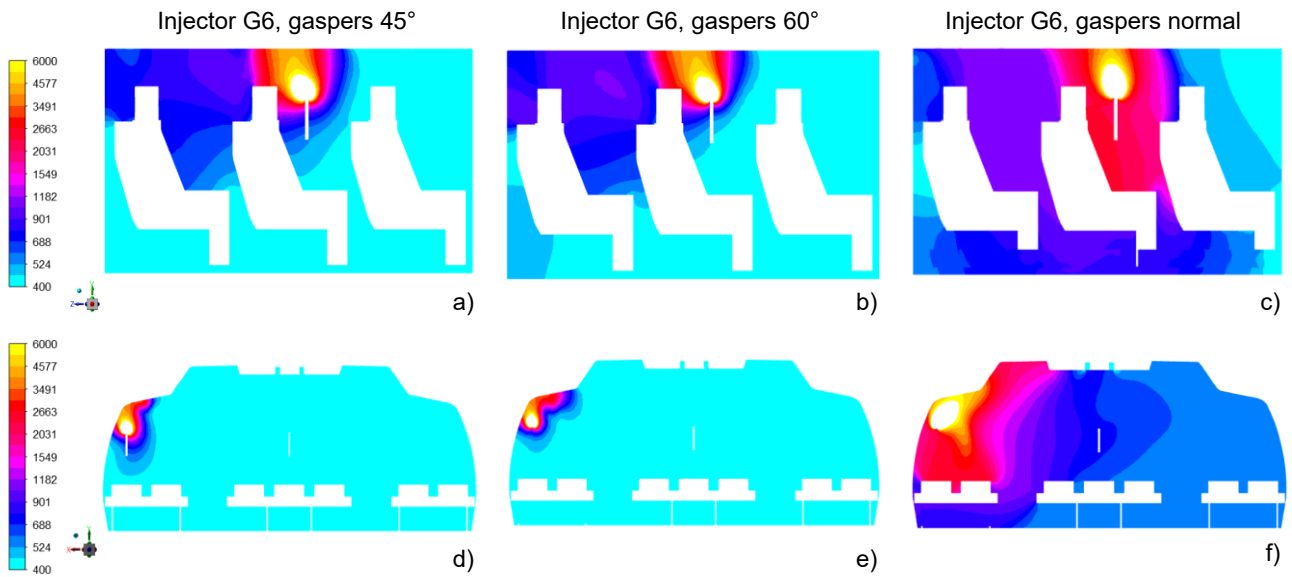


Figure 15 - Gaspers on and injection at G6: molar fraction of CO<sub>2</sub> in ppm at front and side planes.

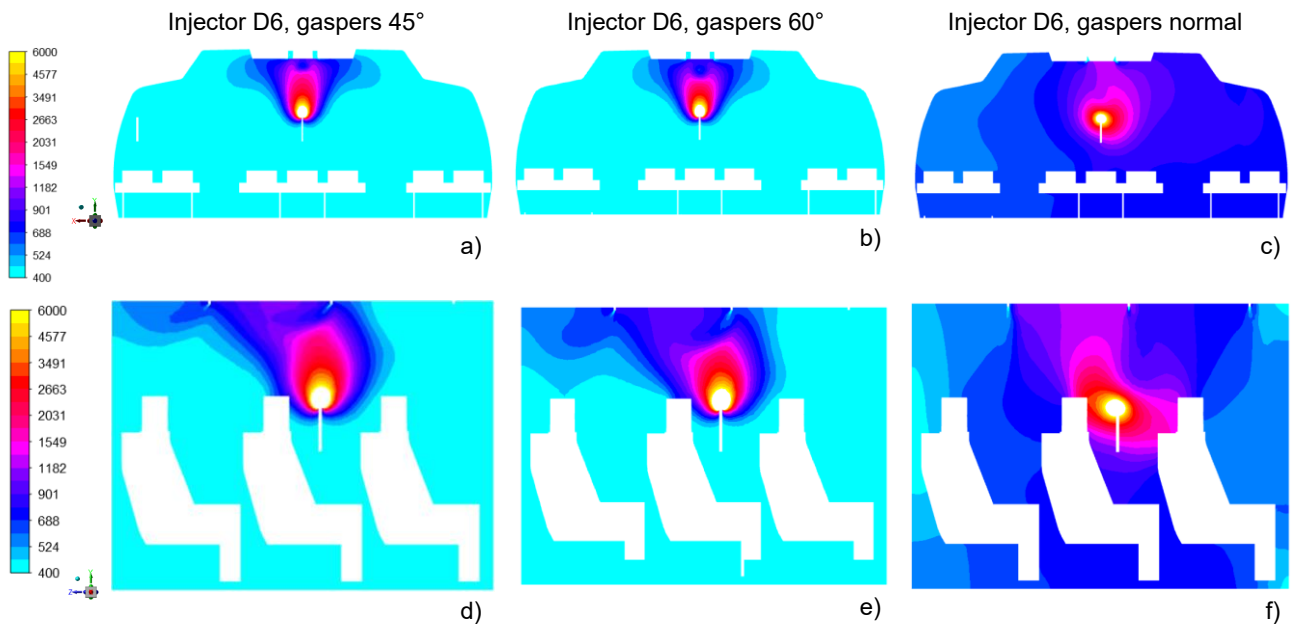


Figure 16 – Gaspers on and injection at D6: comparison of CO<sub>2</sub> molar fractions for different gasper settings at front and side planes.

By analyzing Figure 17 one creates the perception that the gaspers at the baseline experiment were tilted on the side passengers and normal to the surface in the center as shown in b) and g). Finally, when gaspers are normal to the surface, the concentration of CO<sub>2</sub> increases significantly because the upward current caused by thermal plume and the vortex are reduced by the gaspers cold jet. Conjugating these effects, the net result is the decrease of the convection transport which will magnify the diffusion of the contaminant. Further research should be carried out to potentially create a protocol to fix the position of gaspers for the safest position.

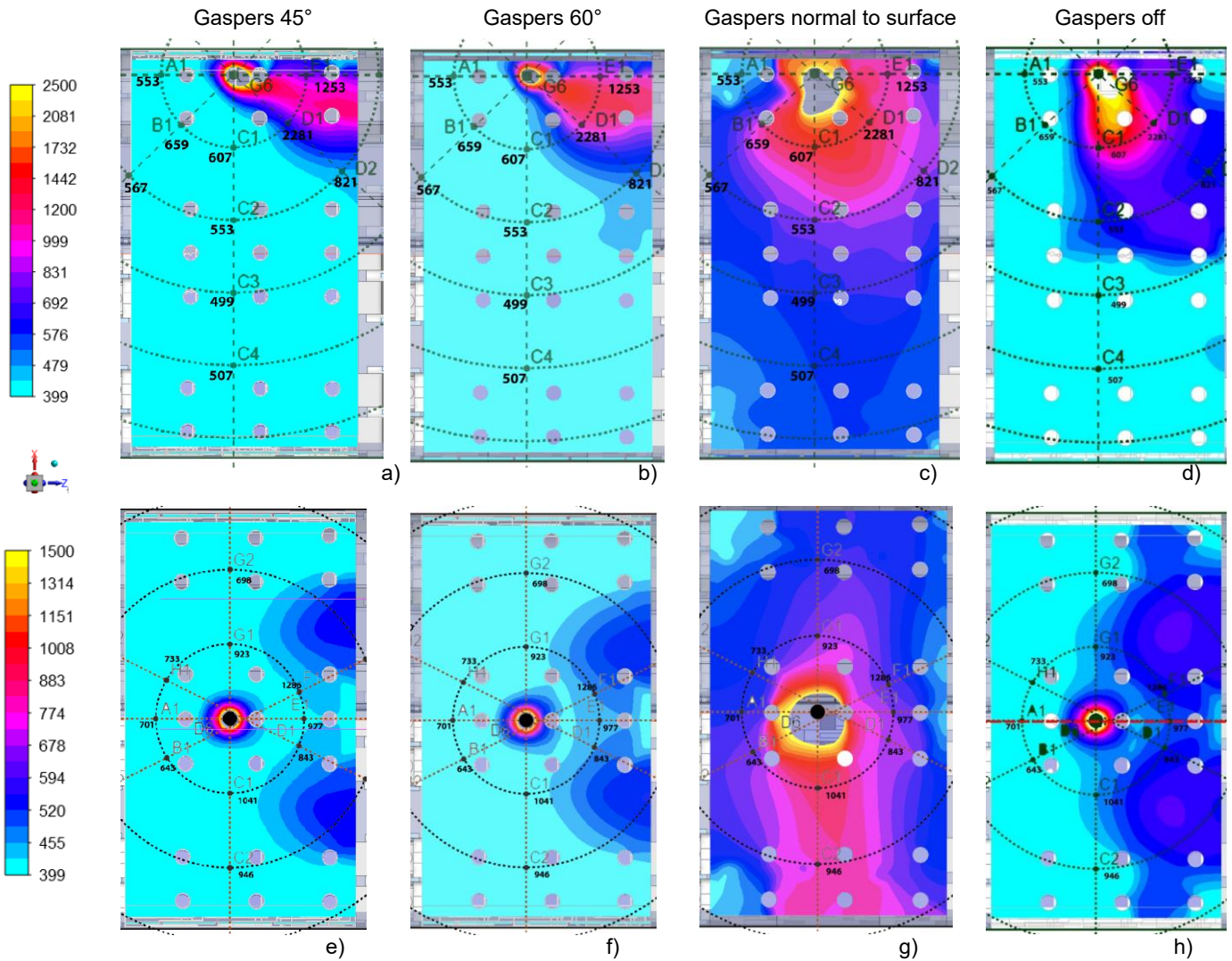


Figure 17 – Comparison of CO<sub>2</sub> molar fractions for different gasper settings at the breathing area.

#### 4. Conclusions

The present work firstly focused on improving the accuracy of the boundary conditions in the aircraft cabin by simulating the complex behavior of the air jets upstream the slot area using a modified RANS realizable  $k-\epsilon$  model, which has demonstrated to produce a good agreement with available experimental data.

The approached established for the air flow simulation subsequently allowed to also simulate a continuous injection source of a contaminant at the center and at the side of the cabin. In the absence of gaspers, the concentration of the contaminant is higher near the ceiling walls due to the thermal plumes.


When gaspers were added, the inclination of the gasper was crucial for determining the fate of the contaminant. By activating the gaspers normal to the ceilings, the combination of the cold jet with the thermal plume leads to a scenario closer to still air, whereas the longitudinal velocity remained small, thus leading to a decrease in longitudinal spread and increasing diffusion.

When gaspers were tilted to the manikin, there is a significant increase in longitudinal velocity without a major decrease in strength of the thermal plume. Furthermore, turning on gaspers reduced the flowrate available to the supply air. This will decrease the strength of the global designed pattern, thus limiting the control the designer intended.

## 5. Acknowledgements

This work has been supported by Fundação para a Ciência e a Tecnologia (FCT), through IDMEC, under LAETA, project UID/EMS/50022/2020.

## 6. Author Contact

**Carlos L. S. Raposo**  <https://orcid.org/0000-0001-8821-6620>,  
email: [carlos.s.raposo@tecnico.ulisboa.pt](mailto:carlos.s.raposo@tecnico.ulisboa.pt)

**João M. M. Sousa**  <https://orcid.org/0000-0002-0310-3115>

## 7. Copyright Statement

The authors confirm that they, and/or their company or organization, hold copyright on all of the original material included in this paper. The authors also confirm that they have obtained permission, from the copyright holder of any third party material included in this paper, to publish it as part of their paper. The authors confirm that they give permission, or have obtained permission from the copyright holder of this paper, for the publication and distribution of this paper as part of the ICAS proceedings or as individual off-prints from the proceedings.

## 8. Appendix

### 8.1 Source Term UDF

```
#include "udf.h"
#define Ck3 0.23
DEFINE_SOURCE(udfsourcek,c,t,dS,eqn)
{
  real x[ND_ND];
  real con, source;
  real rho =C_R(c,t);
  real diss =C_D(c,t);
  C_CENTROID(x,c,t);
  con = Ck3*rho;
  source = con*diss;
  return source;
}
```

## 9. References

- [1] Air Transport Action Group. Waypoint 2050. <https://aviationbenefits.org/environmental-efficiency/climate-action/waypoint-2050/>. Accessed Jan. 9, 2022.
- [2] International Air Transport Association. *Economic Performance of the Airline Industry*. 2021.
- [3] Bourouiba, L., Dehandschoewercker, E., and Bush, J. W. M. “Violent Expiratory Events: On Coughing and Sneezing.” *Journal of Fluid Mechanics*, Vol. 745, 2014, pp. 537–563. <https://doi.org/10.1017/jfm.2014.88>.
- [4] Shehadi, M. F., Hosni, M. H., and Jones, B. W. “Airflow and Turbulence Analysis inside a Wide-Body Aircraft Cabin Mockup.” *Indoor and Built Environment*, Vol. 27, No. 6, 2018, pp. 766–785. <https://doi.org/10.1177/1420326X16689720>.
- [5] Yang, C., Liu, J., and He, F. “Evolution of Large-Scale Flow Structures and Traces of Marked Fluid Particles within a Single-Aisle Cabin Mock-Up.” *Building Simulation*, Vol. 10, No. 5, 2017, pp. 723–736. <https://doi.org/10.1007/s12273-017-0351-6>.
- [6] Mendes, P. J., Pinto, J. F., and Sousa, J. M. M. “A Non-Dimensional Functional Relationship for the Fine Particle Fraction Produced by Dry Powder Inhalers.” *Journal of Aerosol Science*, Vol. 38, No. 6, 2007, pp. 612–624. <https://doi.org/10.1016/j.jaerosci.2007.04.001>.
- [7] Kinahan, S. M., Silcott, D. B., Silcott, B. E., Silcott, R. M., Silcott, P. J., Silcott, B. J., Distelhorst, S. L., Herrera, V. L., Rivera, D. N., Crown, K. K., Lucero, G. A., and Santarpia, J. L. “Aerosol Tracer Testing in Boeing 767 and 777 Aircraft to Simulate Exposure Potential of Infectious Aerosol Such as SARS-CoV-2.” *PLoS ONE*, 2021, pp. 1–19. <https://doi.org/10.1371/journal.pone.0246916>.
- [8] Silcott, D. B., Kinahan, S. M., Santarpia, J. L., Silcott, B. E., Silcott, R. M., Silcott, P. J., Silcott, B. J., Distelhorst, S. L., Herrera, V. L., Rivera, D. N., Crown, K. K., Lucero, G. A., Bryden, W., McLoughlin, M., Cetta, M., and Accardi, R. *TRANSCOM/AMC Commercial Aircraft Cabin Aerosol Dispersion Tests*. 2020.
- [9] Davis, A. C., Zee, M., Clark, A. D., Wu, T., Jones, S. P., Waite, L. L., Cummins, J. J., and Olson, N. A. “Computational Fluid Dynamics Modeling of Cough Transport in an Aircraft Cabin.” *Scientific Reports*, Vol. 11, No. 23329, 2021. <https://doi.org/10.1038/s41598-021-02663-8>.
- [10] Beneke, J. M. *Small Diameter Particle Dispersion in a Commercial Aircraft Cabin*. Kansas State University, 2010.
- [11] Shehadi, M. F. *Experimental Investigation of Optimal Particulate Sensor Location in an Aircraft Cabin*. Kansas State University, 2010.
- [12] Trupka, A. T. *Tracer Gas Mapping of a Beverage Cart Wake in a Twin Aisle Aircraft Cabin*. Kansas State University, 2011.
- [13] Anderson, M. D. *Effect of Gaspers on Airflow Patterns and the Transmission of Airborne Contaminants within an Aircraft Cabin Environment*. Kansas State University, 2012.
- [14] Ebrahimi, K. *Numerical Simulation of Turbulent Airflow, Tracer Gas Diffusion, and Particle Dispersion in a Mockup Aircraft Cabin*. Kansas State University, 2012.
- [15] Shehadi, M. F., Hosni, M. H., and Jones, B. W. “Airflow Distribution in the Longitudinal Plan of a Boeing 767 Mockup Cabin.” *ASME International Mechanical Engineering Congress and Exposition, Proceedings (IMECE)*, Vol. 7, 2014. <https://doi.org/10.1115/IMECE2014-40102>.
- [16] Shehadi, M. F. *Airflow Distribution and Turbulence Analysis in the Longitudinal Direction of a Boeing 767 Mockup Cabin*. Kansas State University, 2015.
- [17] Shehadi, M. F. “Heat Convective Effects on Turbulence and Airflow inside an B767 Aircraft Cabin.” *Fluids*, Vol. 4, No. 3, 2019, p. 167. <https://doi.org/10.3390/fluids4030167>.
- [18] Keshavarz, A., Jones, B. W., Hosni, M. H., and Beneke, J. M. “Experimental Measurements for Gaseous Transport within an Aircraft Cabin.” *Building and Environment*, Vol. 89, 2015, pp. 327–335. <https://doi.org/10.1016/j.buildenv.2015.03.011>.
- [19] Patel, J. A. *Experimental Investigation of Ventilation Effectiveness in an Airliner Cabin Mockup*. Kansas State University, 2017.
- [20] Darrah, I., Bennett, J. S., Jones, B. W., and Hosni, M. H. “Infectious Passenger Isolation System for Aircraft.” *ASHRAE Transactions*, Vol. 125, No. 2, 2019, pp. 288–296.
- [21] Mahmoud, S., Neu, D., Menchaka, K., Shugart, J. M., Hosni, M. H., Mead, K. R., Martin, S. B., McClelland, T., Lindsley, W. G., and Bennett, J. S. “Transport and Containment of Infectious Disease Expelled by Coughing in an Aircraft Cabin.” *ASHRAE Transactions*, Vol. 126, No. 2, 2020, pp. 375–383.
- [22] Mahmoud, S. *Experimental Analysis of Aerosol Dispersion and Containment Solutions in Aircraft Cabins*. Kansas State University, 2021.
- [23] Lin, C.-H., Dunn, K. H., Horstman, R. H., Topmiller, J. L., Ahlers, M. F., Bennett, J. S., Sedgwick, L. M., Wirogo, S., and ASHRAE. “Numerical Simulation of Airflow and Airborne Pathogen Transport in Aircraft Cabins - Part I: Numerical Simulation of the Flow Field.” *ASHRAE Transactions*, Vol. 111, No. 1, 2005, pp. 755–764.

- [24] Lin, C.-H., Horstman, R. H., Ahlers, M. F., Sedgwick, L. M., Dunn, K. H., Topmiller, J. L., Bennett, J. S., Wirogo, S., and ASHRAE. “Numerical Simulation of Airflow and Airborne Pathogen Transport in Aircraft Cabins - Part II: Numerical Simulation of Airborne Pathogen Transport.” *ASHRAE Transactions*, Vol. 111, No. 1, 2005, pp. 764–768.
- [25] Mazumdar, S. *Transmission of Airborne Contaminants of Airliner Cabins*. Purdue University, 2009.
- [26] Poussou, S. B. *Experimental Investigation of Airborne Contaminant Transport by a Human Wake Moving in a Ventilated Aircraft Cabin*. Purdue University, 2008.
- [27] Isukapalli, S. S., Mazumdar, S., George, P., Wei, B., Jones, B. W., and Weisel, C. P. “Computational Fluid Dynamics Modeling of Transport and Deposition of Pesticides in an Aircraft Cabin.” *Atmospheric Environment*, Vol. 68, 2013, pp. 198–207. <https://doi.org/10.1016/j.atmosenv.2012.11.019>.
- [28] Boeing. *767 Airplane Characteristics for Airport Planning*. 2012.
- [29] You, R. *Investigating Airflow Distribution and Contaminant Transport in Commercial Aircraft Cabins*. Purdue University, 2018.
- [30] You, R., Chen, J., Shi, Z., Liu, W., Lin, C.-H., Wei, D., and Chen, Q. Y. “Experimental and Numerical Study of Airflow Distribution in an Aircraft Cabin Mock-up with a Gasper On.” *Journal of Building Performance Simulation*, Vol. 9, No. 5, 2016, pp. 555–566. <https://doi.org/10.1080/19401493.2015.1126762>.
- [31] You, R., Liu, W., Chen, J., Lin, C.-H., Wei, D., and Chen, Q. Y. “Predicting Airflow Distribution and Contaminant Transport in Aircraft Cabins with a Simplified Gasper Model.” *Journal of Building Performance Simulation*, Vol. 9, No. 6, 2016, pp. 699–708. <https://doi.org/10.1080/19401493.2016.1196730>.
- [32] You, R., Chen, J., Lin, C.-H., Wei, D., and Chen, Q. Y. “Investigating the Impact of Gaspers on Cabin Air Quality in Commercial Airliners with a Hybrid Turbulence Model.” *Building and Environment*, Vol. 111, 2017, pp. 110–122. <https://doi.org/10.1016/j.buildenv.2016.10.018>.
- [33] You, R., Zhang, Y., Zhao, X., Lin, C.-H., Wei, D., Liu, J., and Chen, Q. Y. “An Innovative Personalized Displacement Ventilation System for Airliner Cabins.” *Building and Environment*, Vol. 137, No. March, 2018, pp. 41–50. <https://doi.org/10.1016/j.buildenv.2018.03.057>.
- [34] Wang, C., Liu, J., and Zhang, Y. “Accurate Experimental Measurements of Flow Boundary Conditions for Numerical Simulations in an Aircraft Cabin Mockup.” *Indoor Air 2014 - 13th International Conference on Indoor Air Quality and Climate*, No. January, 2014, pp. 803–810.
- [35] Cao, X., Liu, J., Pei, J., Zhang, Y., Li, J., and Zhu, X. “2D-PIV Measurement of Aircraft Cabin Air Distribution with a High Spatial Resolution.” *Building and Environment*, Vol. 82, No. 2012, 2014, pp. 9–19. <https://doi.org/10.1016/j.buildenv.2014.07.027>.
- [36] Li, M., Zhao, B., Tu, J., and Yan, Y. “Study on the Carbon Dioxide Lockup Phenomenon in Aircraft Cabin by Computational Fluid Dynamics.” *Building Simulation*, Vol. 8, No. 4, 2015, pp. 431–441. <https://doi.org/10.1007/s12273-015-0217-8>.
- [37] Liu, M., Chang, D., Liu, J., Ji, S., Lin, C.-H., Wei, D., Long, Z., Zhang, T. T., Shen, X., Cao, Q., Li, X., Zeng, X., and Li, H. “Experimental Investigation of Air Distribution in an Airliner Cabin Mockup with Displacement Ventilation.” *Building and Environment*, Vol. 191, No. January, 2021, p. 107577. <https://doi.org/10.1016/j.buildenv.2020.107577>.
- [38] Mo, H. *Experimental and Computational Study of Interaction of Airflow Inside Aircraft Cabin with Human Body*. Kansas State University, 2002.
- [39] Sun, Y., Zhang, Y., Wang, A., Topmiller, J. L., and Bennett, J. S. “Experimental Characterization of Airflows in Aircraft Cabins, Part II: Results and Research Recommendations.” *ASHRAE Transactions*, Vol. 111, No. 2, 2005, pp. 53–59.
- [40] Ebrahimi, K., Hosni, M. H., and Zheng, Z. C. “Computational Study of Turbulent Airflow in a Full-Scale Aircraft Cabin Mockup - Part I: Determination of Boundary Conditions at the Outlet of Air Diffusers.” *American Society of Mechanical Engineers, Fluids Engineering Division (Publication) FEDSM*, Vol. 1 A, No. July, 2013. <https://doi.org/10.1115/FEDSM2013-16564>.
- [41] Zhang, Z., Chen, X., Mazumdar, S., Zhang, T. T., and Chen, Q. Y. “Experimental and Numerical Investigation of Airflow and Contaminant Transport in an Airliner Cabin Mockup.” *Building and Environment*, Vol. 44, No. 1, 2009, pp. 85–94. <https://doi.org/10.1016/j.buildenv.2008.01.012>.
- [42] Zhang, T. T. *Detection and Mitigation of Contaminant Transport in Commercial Aircraft Cabins*. Purdue University, 2007.
- [43] Zhang, T. T., Li, P., and Wang, S. “A Personal Air Distribution System with Air Terminals Embedded in Chair Armrests on Commercial Airplanes.” *Building and Environment*, Vol. 47, No. 1, 2012, pp. 89–99. <https://doi.org/10.1016/j.buildenv.2011.04.035>.
- [44] Sze To, G. N., Wan, M. P., Chao, C. Y. H., Fang, L., and Melikov, A. “Experimental Study of Dispersion and



- Deposition of Expiratory Aerosols in Aircraft Cabins and Impact on Infectious Disease Transmission.” *Aerosol Science and Technology*, Vol. 43, No. 5, 2009, pp. 466–485. <https://doi.org/10.1080/02786820902736658>.
- [45] Dygert, R. K. *Mitigation of Cross-Contamination in an Aircraft Cabin Through the Use of Localized Exhaust*. Syracuse University, 2010.
- [46] Garner, R. P., Wong, K. L., Ericson, S. C., Baker, A. J., and Orzechowski, J. A. *CFD Validation for Contaminant Transport in Aircraft Cabin Ventilation Flow Fields*. 2003.
- [47] Volavý, F., Fišer, J., and Nöske, I. “Prediction of Air Temperature in the Aircraft Cabin under Different Operational Conditions.” *EPJ Web of Conferences*, Vol. 45, 2013, pp. 1–6. <https://doi.org/10.1051/epjconf/20134501096>.
- [48] Norrefeldt, V., Mayer, F., Herbig, B., Ströhlein, R., Wargocki, P., and Lei, F. “Effect of Increased Cabin Recirculation Airflow Fraction on Relative Humidity, CO<sub>2</sub> and TVOC.” *Aerospace*, Vol. 8, No. 1, 2021, pp. 1–16. <https://doi.org/10.3390/aerospace8010015>.
- [49] Dechow, M., Sohn, H., and Steinhanes, J. “Concentrations of Selected Contaminants in Cabin Air of Airbus Aircrafts.” *Chemosphere*, Vol. 35, Nos. 1–2, 1997, pp. 21–31. [https://doi.org/10.1016/S0045-6535\(97\)00135-5](https://doi.org/10.1016/S0045-6535(97)00135-5).
- [50] Bosbach, J., Heider, A., Dehne, T., Markwart, M., Gores, I., and Bendfeldt, P. *Evaluation of Cabin Displacement Ventilation under Flight Conditions*. 2012.
- [51] Dehne, T., and Bosbach, J. “Comparison of Surface Temperatures and Cooling Rates for Different Ventilation Concepts in an A320 Aircraft Cabin under Flight Conditions.” *Roomvent 2014 13th SCANVAC International Conference on Air Distribution in Rooms*, No. October, 2014.
- [52] Du, X., Li, B., Liu, H., Wu, Y., Cheng, T., and Awbi, H. B. “Effect of Nozzle Air Supply Temperature and Volume Flowrate on the Jet Flow from a Typical Ventilation Nozzle in Aircraft Cabins.” *Indoor and Built Environment*, Vol. 27, No. 4, 2018, pp. 499–511. <https://doi.org/10.1177/1420326X16676881>.
- [53] Fang, Z., Liu, H., Li, B., Baldwin, A., Wang, J., and Xia, K. “Experimental Investigation of Personal Air Supply Nozzle Use in Aircraft Cabins.” *Applied Ergonomics*, Vol. 47, 2015, pp. 193–202. <https://doi.org/10.1016/j.apergo.2014.09.011>.
- [54] Bosbach, J., Kühn, M., Rütten, M., and Wagner, C. “Mixed Convection in a Full Scale Aircraft Cabin Mock-Up.” *ICAS-Secretariat - 25th Congress of the International Council of the Aeronautical Sciences 2006*, Vol. 6, No. June, 2006, pp. 3723–3731.
- [55] Bosbach, J., Pennecot, J., Wagner, C., Raffel, M., Lerche, T., and Repp, S. “Experimental and Numerical Simulations of Turbulent Ventilation in Aircraft Cabins.” *Energy*, Vol. 31, No. 5, 2006, pp. 694–705. <https://doi.org/10.1016/j.energy.2005.04.015>.
- [56] Günther, G., Bosbach, J., Pennecot, J., Wagner, C., Lerche, T., and Gores, I. “Experimental and Numerical Simulations of Idealized Aircraft Cabin Flows.” *Aerospace Science and Technology*, Vol. 10, No. 7, 2006, pp. 563–573. <https://doi.org/10.1016/j.ast.2006.02.003>.
- [57] Chen, W., Liu, J., Li, F., Cao, X., Li, J., Zhu, X., and Chen, Q. Y. “Ventilation Similarity of an Aircraft Cabin Mockup with a Real MD-82 Commercial Airliner.” *Building and Environment*, Vol. 111, 2017, pp. 80–90. <https://doi.org/10.1016/j.buildenv.2016.10.017>.
- [58] Liu, W., Wen, J., Chao, J., Yin, W., Shen, C., Lai, D., Lin, C.-H., Liu, J., Sun, H., and Chen, Q. Y. “Accurate and High-Resolution Boundary Conditions and Flow Fields in the First-Class Cabin of an MD-82 Commercial Airliner.” *Atmospheric Environment*, Vol. 56, 2012, pp. 33–44. <https://doi.org/10.1016/j.atmosenv.2012.03.039>.
- [59] Liu, W., Wen, J., Lin, C.-H., Liu, J., Long, Z., and Chen, Q. Y. “Evaluation of Various Categories of Turbulence Models for Predicting Air Distribution in an Airliner Cabin.” *Building and Environment*, Vol. 65, 2013, pp. 118–131. <https://doi.org/10.1016/j.buildenv.2013.03.018>.
- [60] Cao, Q., Chen, C., Liu, S., Lin, C.-H., Wei, D., and Chen, Q. Y. “Prediction of Particle Deposition around the Cabin Air Supply Nozzles of Commercial Airplanes Using Measured In-Cabin Particle Emission Rates.” *Indoor Air*, Vol. 28, No. 6, 2018, pp. 852–865. <https://doi.org/10.1111/ina.12489>.
- [61] Ebrahimi, K., Zheng, Z. C., and Hosni, M. H. LES and RANS Simulation of Turbulent Airflow and Tracer Gas Injection in a Generic Aircraft Cabin Model. No. 1, 2010, pp. 227–240.
- [62] Padilla, A. M. *Experimental Analysis of Particulate Movement in a Large Eddy Simulation Chamber*. Kansas State University, 2008.
- [63] Lebbin, P. A. *Experimental and Numerical Analysis of Air, Tracer Gas, and Particulate Movement in a Large Eddy Simulation Chamber*. Kansas State University, 2006.
- [64] Research Facilities Navigator. Centre for Air Travel Research (CATR). <https://navigator.innovation.ca/en/facility/national-research-council-canada/centre-air-travel-research-catr>. Accessed May 31, 2022.
- [65] BOEING, Nene, R. R., Moran, B. D., Roberson, D. R., and Braaten, N. T. *Clean Airplane Program – Live Virus*

*Validation Testing*. 2020.

- [66] Müller, R. H. G., Scherer, T., Rötger, T., Schaumann, O., and Markwart, M. “Large Body Aircraft Cabin A/C Flow Measurement by Helium Bubble Tracking.” *Journal of Flow Visualization and Image Processing*, Vol. 4, No. 3, 1997, pp. 295–306. <https://doi.org/10.1615/JFlowVisImageProc.v4.i3.90>.
- [67] Raposo, C. L. S. *Bioaerosol Transport and Sensor in Passenger Aircraft*. Instituto Superior Técnico, 2022.
- [68] ANSYS, I. *ANSYS Fluent Theory Guide*. 2021.
- [69] FreeMapTools. Elevation Finder. <https://www.freemaptools.com/elevation-finder.htm>.
- [70] National Geodetic Survey. Surface Gravity Prediction. [https://geodesy.noaa.gov/cgi-bin/grav\\_pdx.prl](https://geodesy.noaa.gov/cgi-bin/grav_pdx.prl). Accessed Apr. 1, 2022.
- [71] ICAO. “Manual of the ICAO Standard Atmosphere.” 1993.
- [72] Moran, M. J., Shapiro, H. N., Boettner, D. D., and Bailey, M. B. *Fundamentals of Engineering Thermodynamics*. Wiley, 2018.
- [73] Wilke, C. R. “A Viscosity Equation for Gas Mixtures.” *The Journal of Chemical Physics*, Vol. 18, No. 4, 1950, pp. 517–519. <https://doi.org/10.1063/1.1747673>.
- [74] CFD Online. Turbulence Intensity. [https://www.cfd-online.com/Wiki/Turbulence\\_intensity](https://www.cfd-online.com/Wiki/Turbulence_intensity). Accessed May 31, 2022.
- [75] de Tilly, A., and Sousa, J. M. M. “An Experimental Study of Heat Transfer in a Two-Dimensional T-Junction Operating at a Low Momentum Flux Ratio.” *International Journal of Heat and Mass Transfer*, Vol. 51, Nos. 3–4, 2008, pp. 941–947. <https://doi.org/10.1016/j.ijheatmasstransfer.2007.10.012>.
- [76] Melo, M. J., Sousa, J. M. M., Costa, M., and Levy, Y. “Flow and Combustion Characteristics of a Low-NO<sub>x</sub> Combustor Model for Gas Turbines.” *Journal of Propulsion and Power*, Vol. 27, No. 6, 2011, pp. 1212–1217. <https://doi.org/10.2514/1.56286>.